JOURNAL OF GEOPHYSICAL RESEARCH, VOL. 112, D13105, doi:10.1029/2006JD007494, 2007

Regional transport and dilution during high-pollution episodes in southern France: Summary of findings from the Field Experiment to Constraint Models of Atmospheric Pollution and Emissions Transport (ESCOMPTE)

P. Drobinski,[1] F. Saïd,[2] G. Ancellet,[1] J. Arteta,[3] P. Augustin,[4] S. Bastin,[1] A. Brut,[2] J. L. Caccia,[5] B. Campistron,[2] S. Cautenet,[3] A. Colette,[1] I. Coll,[6] U. Corsmeier,[7] B. Cros,[2] A. Dabas,[8] H. Delbarre,[4] A. Dufour,[8] P. Durand,[2] V. Guénard,[5] M. Hasel,[7] N. Kalthoff,[7] C. Kottmeier,[7] F. Lasry,[6] A. Lemonsu,[8] F. Lohou,[2] V. Masson,[8] L. Menut,[9] C. Moppert,[2] V. H. Peuch,[8] V. Puygrenier,[2] O. Reitebuch,[10] and R. Vautard[11]

Received 9 May 2006; revised 30 September 2006; accepted 15 December 2006; published 4 July 2007.

[1] In the French Mediterranean basin the large city of Marseille and its industrialized suburbs (oil plants in the Fos-Berre area) are major pollutant sources that cause frequent and hazardous pollution episodes, especially in summer when intense solar heating enhances the photochemical activity and when the sea breeze circulation redistributes pollutants farther north in the countryside. This paper summarizes the findings of 5 years of research on the sea breeze in southern France and related mesoscale transport and dilution of pollutants within the Field Experiment to Constraint Models of Atmospheric Pollution and Emissions Transport (ESCOMPTE) program held in June and July 2001. This paper provides an overview of the experimental and numerical challenges identified before the ESCOMPTE field experiment and summarizes the key findings made in observation, simulation, and theory. We specifically address the role of large-scale atmospheric circulation to local ozone vertical distribution and the mesoscale processes driving horizontal advection of pollutants and vertical transport and mixing via entrainment at the top of the sea breeze or at the front and venting along the sloped terrain. The crucial importance of the interactions between processes of various spatial and temporal scales is thus highlighted. The advances in numerical modeling and forecasting of sea breeze events and ozone pollution episodes in southern France are also underlined. Finally, we conclude and point out some open research questions needing further investigation.

Citation: Drobinski, P., et al. (2007), Regional transport and dilution during high-pollution episodes in southern France: Summary of findings from the Field Experiment to Constraint Models of Atmospheric Pollution and Emissions Transport (ESCOMPTE), *J. Geophys. Res.*, *112*, D13105, doi:10.1029/2006JD007494.

1. Introduction

[2] Summer atmospheric stagnant air episodes in coastal areas, leading to land/sea breeze flows and associated recirculations of air, have long been recognized as a major factor of development of severe photo-oxidant episodes. Those movements of air masses result from a complex combination of local and mesoscale winds that transport and redistribute pollutants across the air basins, generating exceedances of ozone regulatory thresholds that may recur for several consecutive days when ozone is retained in reservoir at high altitudes. Fast transport of high ozone

[1]Institut Pierre-Simon Laplace, Service d'Aéronomie, Université Pierre et Marie Curie, Paris, France.
[2]Laboratoire d'Aérologie, Université Paul Sabatier, Toulouse, France.
[3]Laboratoire de Météorologie Physique, Université Blaise Pascal, Aubière, France.
[4]Laboratoire de Physico-Chimie de l'Atmosphère, Université du Littoral-Côte d'Opale, Dunkerque, France.
[5]Laboratoire de Sondages Electromagnétiques de l'Environnement Terrestre, Université du Sud Toulon-Var, Toulon, France.
[6]Faculté des Sciences et Technologie, Laboratoire Inter-Universitaire des Systèmes Atmosphériques, Créteil, France.
[7]Institut für Meteorologie und Klimaforschung, Forschungszentrum Karlsruhe, Universität Karlsruhe, Karlsruhe, Germany.
[8]Centre National de Recherches Météorologiques, Météo-France, Toulouse, France.
[9]Laboratoire de Météorologie Dynamique, Institut Pierre-Simon Laplace, École Polytechnique, Palaiseau, France.
[10]Institut für Physik der Atmosphäre, Deutsches Zentrum für Luft- und Raumfahrt, Oberpfaffenhofen, Germany.
[11]Laboratoire des Sciences du Climat et de l'Environnement, Institut Pierre Simon Laplace, Commisariat à l'Énergie Atomique, Gif-sur-Yvette, France.

0148-0227/07/2006JD007494$09.00

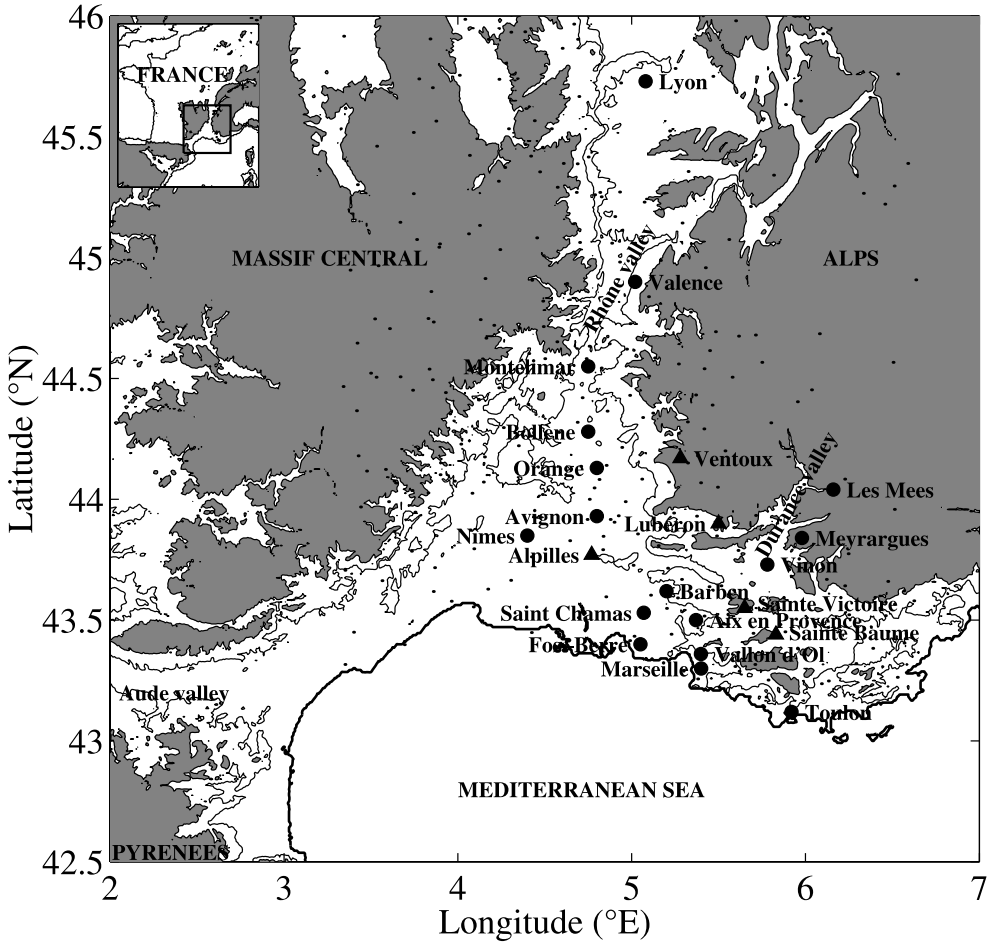

Figure 1. Map of southern France with the topography shaded in grey when higher than 500 m above sea level. The 200 m height isocontour as well as the coastline are shown with thin and thick lines, respectively. Dots indicate the locations of the operational meteorological surface stations operated by Météo-France. The large dots and triangles indicate the locations of cities and of mountain ranges or peaks, respectively. The inset in the upper left corner indicates the region of France shown in the main panel in a square.

concentration to the midtroposphere even frequently occurs when these recirculations are combined with upslope winds in the presence of mountains. Experimental evidence for such phenomena has been reported for large cities of North America [*Rosenthal et al.*, 2003; *Hastie et al.*, 1999] and in Mediterranean areas where strong insolation and low wind speeds provide a favorable environment [*Millán et al.*, 1996; *Ziomas et al.*, 1998], and also on the highly polluted coasts of Asia [*Cheng*, 2002; *Liu et al.*, 2002; *Wang et al.*, 2001].

[3] The study of air quality along the coast of the Provence region (in southern France, see Figure 1) is of particularly interest because of the sea breeze circulation and the presence of the large city of Marseille and its industrialized suburbs (oil refineries in the Fos-Berre area), which emit huge amounts of pollutants into the atmosphere. Subsequent degradation of air quality causes numerous and major pollution episodes especially during summer. This region witnesses a high frequency of photochemical pollution events compared to other French regions within large urban areas, with up to 6 days per month of surface ozone concentrations exceeding 90 ppb during one hour on average.

[4] The other peculiarity of this coastal area is the complexity of topography, combining the coast and the presence of two mountain barriers of different heights (the French Alps to the east that culminates at 4807 m and the Massif Central to the west that culminates at 1885 m), separated by the Rhône valley, a gap of 200 km length and 60 km width. On a southwestern-northeastern axis also lies the Durance valley with a fairly constant width of about 10 km and a length of about 60 km. These topographical features perturb the main sea breeze flow [e.g., *Kusuda and Alpert*, 1983], and put major limitations for numerical weather simulation models with coarse resolution (10–30 km horizontal resolution).

[5] On dynamical aspects, there is a long history of scientific research on the impact of local atmosphere circulations in coastal areas (see, e.g., *Atkinson* [1981] and *Simpson* [1994] for reviews). The land/sea breeze phenomenon is first mentioned in the literature in the 17th century with the work of *Halley* [1686]. The first motivations to the

good understanding of land/sea breeze and its related processes mainly include interests to the fundamental meteorology and its influence on various recreational activities. The first analytical models including Earth rotation effect are developed in 1947 [*Haurwitz*, 1947; *Schmidt*, 1947]. Linear models are then used for analyzing the response of the atmosphere to a differential surface heating [e.g., *Walsh*, 1974; *Rotunno*, 1983] and for scaling the vertical structure of the sea breeze flow [*Steyn*, 1998, 2003] and its horizontal to vertical aspect ratio [*Rotunno*, 1983; *Niino*, 1987; *Dalu and Pielke*, 1989]. The major limit of linear models is the absence of feedback between temperature and wind fields, causing a maximum perturbation at the shoreline. This limit is stepped over by the use of two-dimensional non linear numerical models [e.g., *Estoque*, 1962; *Feliks*, 1993, 2004] followed by their three-dimensional version [e.g., *Bechtold et al.*, 1991]. The initial academic motivation is then progressively replaced by economic and public health interests since breeze circulations are known to contribute to matter and energy transport, and to affect pollution ventilation, species concentration and inland pollutant transport [e.g., *Lyons and Olsson*, 1973]. As an example, *Kolev et al.* [1998, 2000], *Murayama et al.* [1999], and *Vijayakumar et al.* [1998] assess the influence of the sea breeze on the properties of aerosols in coastal regions while *Klemm et al.* [1998] show that in the Athens region, sea breeze air masses entering the city can carry some aged pollution having undergone at least several hours of photochemical processing in the atmosphere. *Schultz and Warner* [1982] find that the ventilation of pollution across the domain of the Los Angeles Basin in the absence of a synoptic-scale wind is strongly influenced by the location of the sea breeze front and the particular stage of the sea breeze life cycle. External processes such as synoptic forcing or orography are shown to affect the dynamics of the sea breeze [*Kitada et al.*, 1986]. Thus *Wakimoto and McElroy* [1986] show that the combination of upper level winds, orographic effects and thermally induced changes in the depth of the planetary boundary layer (PBL) leads to the formation of elevated pollution layers and possible incorporation of pollutants into long-range transport.

[6] On air quality aspects, several coastal cities have been studied, Tokyo, Los Angeles, and Athens in Europe. The main air pollution crossroads over the Mediterranean have also been investigated in the frameworks of several European projects like Meso-meteorological Cycles of Air Pollution in the Iberian Peninsula (MECAPIP) in Spain [*Millán et al.*, 1996], Photochemical Activity and Solar Ultraviolet Radiation (PAUR) in Italy and Greece [*Zerefos et al.*, 2002], or Mediterranean Intensive Oxidant Study (MINOS) in Crete [*Lelieveld et al.*, 2002]. However, the specificity of these sites make it difficult to generalize the major findings of each study. In France, major investigations of air quality in continental cities have also been carried out, such as for Paris in the framework of the Étude et Simulation de la Qualité de l'air en Ile-de-France (ESQUIF) experiment held between 1998 and 2000 [*Menut et al.*, 2000; *Vautard et al.*, 2003a] where it was found that ozone episodes are largely due to large-scale advection from Northern Europe regions, and that local dynamical forcing does not play a major role. In the case of the Marseille area it is not expected that such a transport dominates.

[7] During summer 2001, meteorological and chemical measurements were taken in southern France in the framework of the Field Experiment to Constraint Models of Atmospheric Pollution and Emissions Transport (ESCOMPTE) [*Cros et al.*, 2004] and its urban boundary layer (UBL) subprogram UBL/ESCOMPTE dedicated to the study of the urban boundary layer in the Marseille area (Figure 1) [*Mestayer et al.*, 2005]. This campaign lasted nearly 6 weeks from 7 June to 16 July 2001 and aimed at collecting a large amount of measurements from in situ, passive, and active remote sensors to document the four-dimensional state of the atmosphere over both meteorological and chemical aspects, and understand the precursors of photochemical pollution in the region. Among the ESCOMPTE objectives [*Cros et al. 2004*], the mesoscale transport and dilution (MTD) program was designed to improve the understanding and forecasting of the life cycle of the sea breeze, including its three-dimensional structure and associated contribution to transport and mixing of pollutants emitted from the Marseille and Fos-Berre areas. The questions addressed within the MTD working group were sorted as a function of the temporal and spatial scales.

[8] 1. At synoptic scale, can a part of the temporal and spatial variability of pollutants in the ESCOMPTE target area be attributed to large-scale transport?

[9] 2. At the mesoscale, how do land and sea breezes affect the diurnal redistribution of pollutants? Can the Rhône and Durance valleys modify the sea breeze characteristics and consequently the pollutant distribution? Do slope winds (anabatic and katabatic winds) contribute significantly to pollutant ventilation?

[10] 3. At local scale, does the coastline shape have an impact on sea/land breeze circulation and transport? Does the urban area contribute to local-scale circulations (e.g., urban breezes) or/and disrupts the mesoscale land and sea breeze circulations?

[11] The objective of this paper is to give an overview of the key findings, after five years of research, on the physical and chemical processes leading to summertime atmospheric pollution episodes in southern France, in the light of the innovative measurements collected during the campaign and the use of fine-scale numerical mesoscale and chemistry transport models. After this introduction, section 2 lists the pros for selecting the region of Marseille/Fos-Berre as a target area for pollution studies during ESCOMPTE and the main scientific objectives. It also gives a summary of the ESCOMPTE intensive observation periods (IOPs). Section 3 presents the main challenges identified before the field experiment to be addressed in terms of observation and modeling. Section 4 synthesizes the main findings in terms of observation, numerical simulation and theory of sea breeze and related pollution transport and dilution. Finally, section 5 concludes this overview of results and points out some open research questions needing further investigation.

2. Southern France as a Target Area for Pollution Studies

2.1. Scientific Motivation

[12] A 120×120 km^2 area around the city of Marseille and the Berre pond, in southern France, has been selected to host the ESCOMPTE field campaign (Figure 1). The

selection criteria were based upon strong pollutant sources (urban and industrial) within the experimental area, high occurrence of photochemical pollution events and the presence of a dense, operational pollution monitoring network. This area best fulfills these criteria.

[13] This area is constituted by three different zones: (1) the urban area of Marseille with 1.2 million inhabitants, (2) the Fos-Berre zone around a pond located 15 km northwest of Marseille and separated from the city by 300 m high hills, which is characterized by a strong industrial zone (refineries, power plants, etc.) surrounded by residential areas with important traffic, and (3) rural areas either agricultural or covered by Mediterranean natural landscape.

[14] The atmospheric circulation over this area is highly influenced by orography. On a large scale the Alps and Massif Central at times reinforce in the Rhône valley a strong northerly flow called Mistral [*Caccia et al.*, 2004; *Corsmeier et al.*, 2005; *Drobinski et al.*, 2005; *Guénard et al.*, 2005]. On a smaller scale, the ranges of smaller mountains parallel to the coastline (i.e., Sainte Baume, Sainte Victoire, Luberon, Mont Ventoux) tend to channel the air masses in a west-east manner. The sea-land contrasts induce sea breeze during daytime, with advection of marine air masses as far as 100 km inland.

2.2. Brief Description of the Synoptic Environment of the Documented Sea Breeze Cases

[15] The period and the area of the ESCOMPTE campaign were particularly favorable to the development of photochemical pollution events. During the studied month, no less than 11 days were affected by atmospheric pollution [*Cros et al.*, 2004]. IOP 1 covered 14 and 15 June. These two days have to be considered as a test for the whole ESCOMPTE experimental setup; 15 June was well documented with eight aircraft flights, characterized by cloudy conditions, a thin boundary layer, and low pollution levels. IOP 2 started on 21 June and ended on 26 June. It was decided to split this IOP into two contiguous parts, called 2a and 2b, since meteorological conditions changed significantly on 23 June at 1700 UTC. IOP2a corresponds to the end of a Mistral situation with a moderate northwesterly to westerly wind, clear skies, hot temperature (>30°C). The Marseille and Fos-Berre plumes then extended toward the east and over the sea. The highest surface ozone concentrations were observed near Toulon, in the easternmost part of the ESCOMPTE domain. IOP2b best characterizes a pollution event. During three windless days, temperature (>34°C) and surface ozone concentration reached high values (125 ppb all around Aix en Provence on 24 June; 100 ppb over the whole domain and up to 150 ppb in the Durance Valley on 25 June; 115 ppb in the Rhône valley on 26 June with a light southerly wind). This episode was heavily documented. IOP 3 started on 2 July and ended on 4 July and was a short but interesting episode, characterized by a sea breeze interacting with a large-scale flow veering from the northwest to the southwest in altitude and blowing from the south/southwest near the surface. On the last day, the southwesterly wind became stronger and cloudiness appeared on the domain. The last IOP (IOP 4), starting on 10 July and ending on 13 July, was launched under hot temperature and clear sky conditions but with a westerly/northwesterly synoptic wind that prevented the accumulation of pollutants.

3. Challenges for New Measurements and Modeling Tools

3.1. Observation Network

[16] During ESCOMPTE, aircraft flights, together with tethered and constant volume balloons (CVBs), radiosonde systems and remote sensing measurements, and associated with the continuous surface measurements, provided the most comprehensive picture of atmospheric dynamics and chemistry over a wide range of relevant spatial and temporal scales in the French Mediterranean area. An extensive description of the instrumental setup, with the location of all instruments, is given by *Cros et al.* [2004]. The instrumental setup was designed in order to document the main sea breeze features and their modulation by the regional complex topography and the urban area and to relate them to ozone distribution.

[17] Since the sea breeze is driven by horizontal gradient of surface temperature and heat fluxes, the instrumental setup relied considerably on a dense network of surface meteorological stations. For ESCOMPTE, the already dense network of conventional meteorological surface stations (operated by Météo-France) was completed with 14 additional stations (measuring pressure, temperature, relative humidity, wind speed and direction, short wave and/or total radiation measurements). In addition, the surface energy budget was measured in nine of these stations. Temperature and relative humidity were also measured onboard three mobile cars at rural sites, and on an UBL network of 20 sensors spread over Marseille agglomeration [*Mestayer et al.*, 2005]. This extremely dense station network was necessary to resolve small-scale features and to achieve the same resolution for observational data as for numerical weather prediction and research models, which was essential for the validation of these models. The vertical structure of the sea breeze was documented by a tethered balloon (measuring pressure, temperature, water vapor content, wind speed and direction, and ozone concentration, from the ground up to 200 m), conventional radiosoundings and a large deployment of active remote sensors like Doppler lidars, sodars, UHF wind profilers (16 in total) in the city of Marseille, in semiurban and rural zones. During ESCOMPTE, the use of the airborne Doppler lidar WIND (Wind Infrared Doppler lidar) on board the German Falcon 20, opens the additional spatial dimension of the aircraft's track and allows the retrieval of the wind field in a two-dimensional plane in the clear air or partially cloudy atmosphere. The data set provided by the airborne Doppler lidar allows a unique insight on the three dimensional structure of the sea breeze including its inland penetration, its depth and intensity and the perturbation by the complex terrain of its main features [*Drobinski et al.*, 2006]. In addition to the Falcon 20 flights, the measurements of the mean and turbulent meteorological variables in the PBL were provided by three French research aircraft (Fokker 27 ARAT, Merlin IV and Piper Aztec 23) and two additional German research aircrafts (Dornier 128 and microlight research aircraft) performing classic dynamical, thermody-

namical and air chemical slow and fast measurements [*Saïd et al.*, 2005].

[18] The surface ozone concentration was documented by the stations operated by the local air quality networks AIRMARAIX and AIRFOBEP completed by 18 continental surface stations used to follow the pollutant plumes and 2 stations onboard of ships used to obtain information on the chemical conditions at the outskirts of the ESCOMPTE region and monitor atmospheric chemistry over the sea. The vertical profiles of ozone concentration were observed by 4 ground-based ozone lidars. Several precise locations were defined, combining a wind profiler (Doppler lidar, radar, or sodar) with an ozone lidar, in order to create a multiscale (local and regional) remote sensing network on emission zones where photochemical processes are dominant, on intermediate zones where ozone is mainly generated by transport processes, and on rural zones in order to give information on the domain limits. Intercomparison of ozone measurements was performed at the beginning of the field campaign to assess the global measurement uncertainties [*Fréjafon et al.*, 2005]. The measurements of the meteorological and chemical variables within the PBL were also provided by the aircrafts (except the Falcon 20) equipped for chemical measurements such as NO_x, NO_y, O_3, CO, or CO_2, radiation measurements including the NO_2 photolysis rate JNO_2. Some of these aircrafts measured chemical species fluxes. CVBs were also used to follow pollutant plumes, and to investigate the evolution of the plume thermodynamics and chemical properties in a "Lagrangian mode".

3.2. Numerical Modeling

[19] The main objectives of the numerical modeling efforts made in the context of ESCOMPTE were (1) to document the capability of state-of-the-art meso-γ-scale numerical models to simulate air flow and of chemistry-transport models to predict chemical species fields in complex terrain and (2) to improve the process understanding of the underlying interactions between atmospheric processes and pollutant distribution. The specific research challenges were (1) to simulate the detailed characteristics and evolution of the sea breeze flow in complex orography and to better understand the underlying flow dynamics, (2) to diagnose accurately the PBL depth at the transition between land and sea where it evolves sharply over a small horizontal range and affects the estimation of the pollutant dilution, (3) to determine the complex interactions between surface emissions and ozone production with respect to the meteorological conditions, and (4) to quantify the impact of simulated meteorological field inaccuracies on the production rate and concentration of ozone. Necessary ingredients for a high forecasting skill of high-resolution numerical models for weather and air quality are expected to be (1) an accurate simulation of larger-scale aspects (the sensitivity of the local response of the sea breeze to any uncertainty in the large-scale analysis is large because of the weakness of the sea breeze intensity), (2) a good initial analysis of the low-level atmospheric state (to account for small-scale surface heterogeneities), and (3) a high-resolution model with a proper representation of orography and urban area and sophisticated parameterizations for physical processes like radiation and turbulence. Moreover, the uniquely dense data set collected during ESCOMPTE was expected to offer one of the first opportunities to clearly demonstrate the possible benefits of future real-time meso-γ-scale numerical prediction of the weather and air quality.

[20] Different dynamical and chemical models have been used to analyze the ESCOMPTE database. The main dynamical models are the nonhydrostatic mesoscale models Méso-NH [*Lafore et al.*, 1998], MM5 [*Dudhia*, 1993] and RAMS (Regional Atmospheric Modeling System) [*Cotton et al.*, 2003]. Some of these models are coupled online with chemistry models. This is the case of Méso-NH (also called Méso-NHC) which includes a chemistry module and RAMS which is coupled online with a condensed chemistry model (MOCA) including 29 species [*Aumont et al.*, 1996]. All these models have been run with horizontal scale spanning from 250 m to 5 km and several nested grids. The MM5 model has also been used to force the chemistry transport model CHIMERE [*Schmidt et al.*, 2001; *Vautard et al.*, 2003b]. The operational weather forecast models of Météo-France ARPEGE (typical mesh size of 30 km) and ALADIN (typical mesh size of 10 km) have been used to force the chemistry transport model MOCAGE [*Dufour et al.*, 2005; *Michou et al.*, 2005]. All these models use an emission inventory which was designed for the purpose of the ESCOMPTE program and built following a bottom-up approach with a 1 km resolution [*Franois et al.*, 2005]. It notably describes the emissions of 95 gaseous compounds involved in ozone production, while biogenic emissions, including isoprene and alpha-pinene, have been hourly calculated using meteorological ambient parameters. The comparison of the dynamical and chemical models with the extensive ESCOMPTE database has been the subject of an international modeling exercise between 2004 and 2006. The results of this intercomparison are available on http://medias.obs-mip.fr/escompte/exercice/HTML/exe.html.

4. Key Findings

4.1. Large-Scale Contribution to Local Ozone Distribution

[21] In the PBL, the afternoon development of local pollution plumes is observed almost every day with a large spatial variability caused by the complex local atmospheric circulation, discussed in the following section, and a large surface heterogeneity of the emission sources. Conversely, above the PBL, the spatial variability is much smaller, indicating the large horizontal extent of layers presenting an excess or a depletion of ozone. As an illustration, Figure 2 shows the time evolution of the vertical profile of ozone measurements on 21 June (IOP2a) and 26 June (IOP2b) by two ozone lidars located 30 km apart, at Aix les Milles (near Aix en Provence) and Saint Chamas. Below about 1500 m height, small timescale variability can differ from one location to the other whereas in the free troposphere, a broad agreement is found, meaning that similar air masses are sampled by the two lidars. Thus, above the PBL, the ozone concentration variability is driven by dynamical processes at large scales (typically larger than 50 km) while smaller-scale variability in the PBL is due the mesoscale circulations [*Ancellet and Ravetta*, 2005]. *Dufour et al.* [2005] show that providing their own time-dependent consistent boundary conditions,

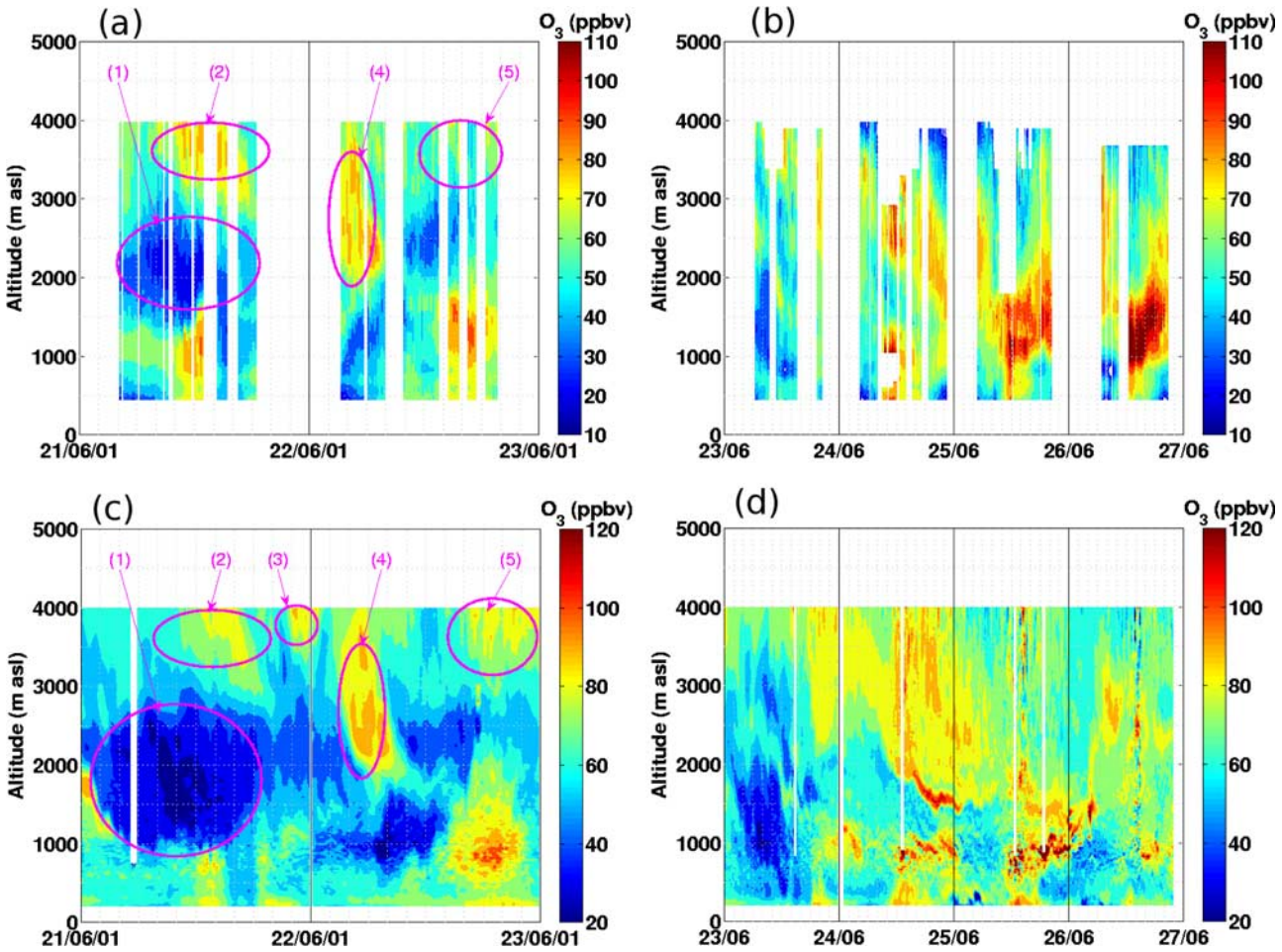

Figure 2. Vertical profiles of ozone concentration as a function of time measured by two DIAL ozone lidars during (a and c) IOP 2a and (b and d) IOP 2b: the ALTO ozone lidar located at Aix les Milles (Figures 2a and Figures 2b) and the EPFL ozone lidar located at Saint Chamas, 30 km west of Aix les Milles (Figures 2c and 2d). Adapted from *Ancellet and Ravetta* [2005] and *Simeonov et al.* [2004].

chemistry transport models are able to account for most of the complex vertical and horizontal structures documented during ESCOMPTE.

[22] In order to assess the dynamical processes responsible for the ozone variability in the free troposphere, numerical modeling and lagrangian studies were conducted by *Dufour et al.* [2005], *Cousin et al.* [2005], and *Colette et al.* [2006] for IOP2, during which typical types of weather were observed. These studies showed that during IOP2, long-range transport but also stratospheric intrusions contribute to the high variability over the whole tropospheric column, consistent with results from PAUR and MINOS projects [*Lelieveld et al.*, 2002; *Zerefos et al.*, 2002; *Traub et al.*, 2003]. In detail, back trajectories were computed from the location of the ozone lidar located at Aix les Milles using the FLEXPART lagrangian particle dispersion model for synoptic-scale processes, and the nonhydrostatic model Méso-NH for mesoscale processes [*Colette et al.*, 2006]. For IOP2a (21 and 22 June), synoptic-scale processes above the Northern Atlantic region drive the observed ozone variability whereas during IOP2b (23–26 June), most free tropospheric air masses come from the PBL of the Iberian peninsula.

[23] To analyze the synoptic-scale processes above the Atlantic Ocean during IOP2a, air masses following similar trajectories were clustered in different groups. Consistence is found between these coherent ensembles of trajectories and the observed ozone variability. So each ozone anomaly (see ellipses in Figures 2a and 2c) can be assign to a specific transport pathway. The ozone depleted layer indicated by (1) corresponds to air masses transported in a warm conveyor belt (WCB) on 17 June associated with a surface low centered at (32°W, 50°N). Its low ozone content is in good agreement with an origin above the marine PBL. The air masses indicated by (2) and (4) are advected in the vicinity of a deep cutoff low active on 19 June in the Azores region (25°W, 42°N). The potential vorticity along the mesoscale trajectories corresponding to these air masses, is higher than the surrounding potential vorticity suggesting that they correspond to stratospheric streamer. The high ozone levels measured for these air masses is thus of stratospheric origin. The rich ozone layer (3) is associated with a WCB active above the northeastern USA. However, after having undergone a strong ascent, these air masses are advected in the tropopause region before reaching the measurement site. Consequently, it is not clear whether these high ozone

concentrations are related to an anthropogenic or stratospheric source. Finally, the stratospheric origin of the observed high ozone concentrations indicated by (5) is related to a strong subsidence in a trough off the shore of Portugal on 19 and 20 June. These air masses are thus coming from the tropopause region.

[24] After 23 June, the ozone variability in the free troposphere above the ESCOMPTE region is driven by transport

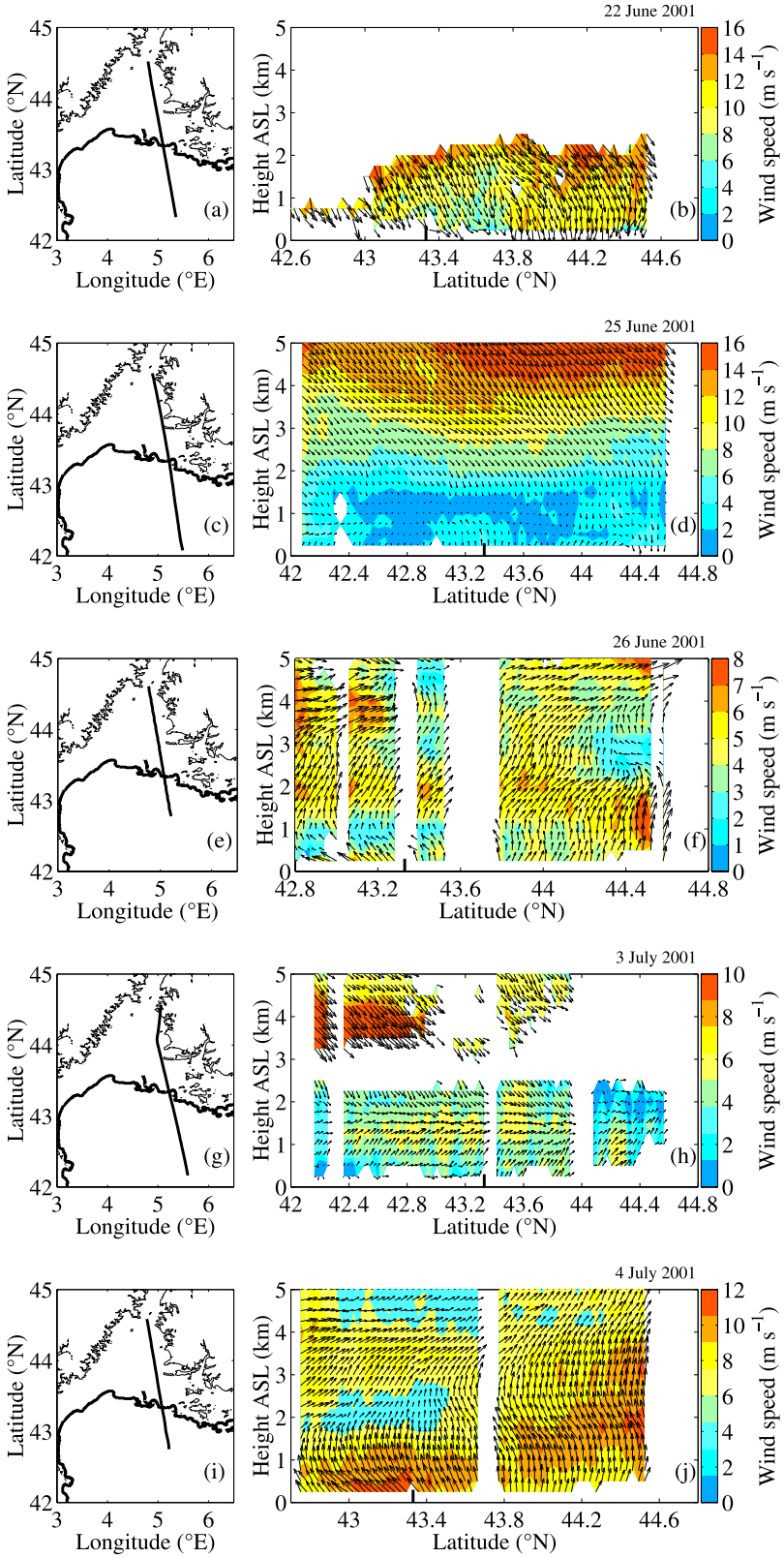

Figure 3

processes above the European continent. A thermal low develops every day above the Iberian Peninsula which favors the onset of orographic and sea breezes and shallow convection. A trough stagnates above southwestern Europe so that air masses exported from the Iberian PBL can be advected to the ESCOMPTE area. The lagrangian trajectories suggest that between 23 and 26 June, 33% of the air masses arriving between 2000 m and 5000 m asl in the ESCOMPTE region come from the Iberian PBL, which is slightly more than during MINOS (23%) [*Traub et al.*, 2003] but still consistent considering the small number of days analyzed during ESCOMPTE and MINOS. Air masses remaining in the free troposphere during the three days preceding their arrival in the ESCOMPTE area, are associated with low ozone content in the free troposphere, especially in the morning of 23 June, around 2000 m on 24 June, and above 3500 m on 25 and 26 June (see Figures 2b and 2d). The ozone rich air masses having left the PBL less than 5 hours before being observed by the lidar at Aix les Milles come from the ESCOMPTE area. Their time and altitude of arrival above the lidar are consistent with those expected for the Marseille and Fos-Berre pollution plumes, lifted above the PBL. The other air masses leaving the PBL several hours before arriving in the ESCOMPTE region, come from the PBL of the Iberian peninsula. The pattern of these air masses is strongly correlated with the high ozone values measured by the lidar in the free troposphere. This finding illustrates how thermal and convective processes in the Iberian peninsula followed by intra-European transport can explain tropospheric ozone variability in the ESCOMPTE region.

[25] These tropospheric ozone layers in the ESCOMPTE region are not expected to be reintegrated in the southerly/southwesterly near-surface sea breeze flow blowing within the PBL via the upper level return flow of the sea breeze (expected to blow from the north). Indeed, as illustrated in Figure 3, showing the wind field below the Falcon 20 flight track along the Rhône valley, one key feature found during ESCOMPTE is that the return flow of the textbooks on sea breeze circulation is very seldom seen in this area [*Drobinski et al.*, 2006]. This is due to (1) the presence of a systematic non zero background wind which prevails over the return flow which is expected to be much weaker than the sea breeze flow [see *Rotunno*, 1983, Figure 2] and (2) the three-dimensional structure of the sea breeze caused by complex coastline shape. The absence of a marked return flow in this area can question the reentry of the pollutants with the sea breeze few days later as suggested by *Millán et al.* [1996] from the analysis of the measurements collected during MECAPIP project in the eastern coast of the Iberian peninsula (mechanism called ''photochemical reactor'').

4.2. Mesoscale Horizontal Transport by the Sea Breeze in the PBL

[26] Studies of PBL transport processes show that during pollution episodes, the sea breeze can export inland the pollutants emitted from the Marseille urban area and the Fos-Berre plants, and that the countryside is often more polluted than the area immediately surrounding the pollutant sources. Table 1 illustrates this point. It shows that ozone concentration is low at Marseille and higher at Aix en Provence (30 km north of Marseille, see Figure 1) under pure sea breeze conditions (25 and 26 June, i.e., IOP2b, and 3 and 4 July, i.e., IOP3), leading to photochemical pollution. Ozone builds up from morning emissions the plume while being advected inland by the afternoon sea breeze. In Provence, the sea breeze shares its occurrence with the Mistral which is frequently observed to extend as far as a few hundreds of kilometers from the coast and is thus associated with low pollution levels in Provence as the Mistral advects the pollutants away from their sources of emission over the Mediterranean. Table 1 shows that the ESCOMPTE Mistral events correspond to low ozone concentration over the region, with one exception on 1 July when the ozone concentration is higher than usual because high-level tropospheric ozone is incorporated within the Mistral flow [*Corsmeier et al.*, 2005]. During IOP2a, a Mistral event occurs, but its weak intensity allows the sea breeze to break through during daytime. Because of the adverse Mistral flow, the sea breeze cannot penetrate far inland making the pollutants accumulate close to the coastline near the emission sources [*Bastin et al.*, 2006] (Table 1). The dilution of ozone during its transport inland is modulated by the variation of the PBL depth along the polluted air mass trajectory. The observations and simulations of all ESCOMPTE IOPs allow to draw some robust conclusions on the structure of the PBL in the ESCOMPTE target area for the different synoptic conditions encountered during the field campaign. The sea breeze penetrates inland associated with the development of an internal PBL at the transition between sea and land. The advection of cold marine air by the sea breeze maintains a shallow PBL (about 0.5 km depth) close to the shore while farther inland the PBL depth can reach typical values of summer continental PBL in the plain (i.e., about 1.5–2 km) and sometimes even larger values over the mountains where anabatic slope winds contribute to the PBL vertical extension [*Kalthoff et al.*, 2005; *Saïd et al.*, 2007].

4.2.1. Near-Surface Ozone Transport

[27] A detailed description of the sea breeze evolution and the associated ozone transport is shown in Figures 4 and 5 for the two typical days of the ESCOMPTE campaign (22 June, i.e., IOP2a, and 25 June, i.e., IOP2b). The impact of the sea breeze on ozone concentration is clearly

Figure 3. (a, c, e, g, and i) Topography of the ESCOMPTE area. The thin and thick lines indicate the 500-m isoline and the coastline, respectively. The thick segment represents the flight track of the DLR Falcon 20 along which the vertical cross section of the horizontal wind field from the WIND data is extracted and shown in Figures 3b, 3d, 3f, 3h, and 3j. (b, d, f, h, and j) Vertical cross section of the horizontal wind field from the WIND data along the leg shown in Figures 3a, 3c, 3e, 3g, and 3i on 22, 25, and 26 June 2001 and 3 and 4 July 2001. Arrows indicate the horizontal wind speed and direction as a function of height, and the superimposed color indicates the wind speed. The absence of data corresponds to discarded unreliable data. The dark thick tick mark indicates the location of the coast. Adapted from *Drobinski et al.* [2006].

Table 1. Ozone Concentration Measured and Simulated With CHIMERE at Marseille and Aix en Provence and Averaged Between 1000 and 1600 UTC, as a Function of the Type of Atmospheric Circulation Regime[a]

Date	Flow Regime	Measured Ozone Concentration, ppb	Simulated Ozone Concentration, ppb	Sea Breeze Inland Penetration, km
17 Jun	M	38.0/41.2	—/—	—
18 Jun	M	40.5/42.2	—/—	—
19 Jun	M	42.0/43	—/—	—
21 Jun (IOP2a)	M + SB	70.0/49.8	69.6/63.8	20
22 Jun (IOP2a)	M + SB	57.5/55.0	74.9/62.1	30
23 Jun (IOP2a)	M + SB	60.0/42.2	67.2/60.4	30
24 Jun (IOP2b)	M (end) + SB	50.0/95.9	71.9/81.1	80
25 Jun (IOP2b)	SB	31.0/74.3	74.3/91.2	100
26 Jun (IOP2b)	SB	46.0/75.5	81.6/80.3	120
28 Jun	M	44.0/43.8	—/—	—
1 Jul (IOP3)	M	50.5/49.8	60.8/59.7	—
3 Jul (IOP3)	SB	50.0/75.6	77.2/74.6	110
4 Jul (IOP3)	SB	45.5/67.8	65.8/72.8	150

[a]The left number is Marseille, and the right number is Aix en Provence. M stands for "mistral," and SB stands for "sea breeze". The sea breeze inland penetration in the Rhône valley, when it exists, is indicated in the last column. The CHIMERE simulations were conducted for the IOPs only.

visible in Figures 4 and 5 which display the surface ozone concentration and 10 m wind speed and direction on 22 and 25 June at 0600, 0900, 1200, 1500 and 1800 UTC simulated using the MM5 mesoscale model coupled with the chemistry transport model CHIMERE.

[28] CHIMERE outputs were carefully compared with observations of CO, O_3 and NO_2, at the ground level and in altitude [*Lasry*, 2006]. Comparison of modeled values with airborne measurements indicate that the CO regional background is accurately reproduced by CHIMERE, as well as the location and amplitude of local peaks, while only minor disagreements are observed (Figure 6). Ozone time series (Figure 7) reveal that CHIMERE is able to reproduce the change in the ozone behavior inland between IOP2a and IOP2b (Le Pontet, close to Avignon), the modeled rural background, and the intensity and shape of the peaks inland (Salon de Provence). Nocturnal ozone titration is less accurately predicted since it is often of very local origin. Figure 7 also illustrates the overestimation in urban areas (Marseille), the underestimation of the ozone maximum at Aix on 24 June (observed for many models during the ESCOMPTE modeling exercise), and the missed peaks at the northernmost sites (Mourre Negre) which result from slight deviations of the direction of the wind that transports too far to the east the secondary plume. Because of its short lifetime, NO_2 is difficult to reproduce in Eulerian models. Nevertheless, time series in Figure 8 indicate that the order of magnitude of the modeled NO_2 mixing ratios is correct, as well as the evolution in concentrations from urban to rural sites, and from IOP2a to IOP2b in inland sites due to the presence of the see breeze.

[29] Just after sunrise on 22 June, the Mistral transports the primary pollutants, emitted near the coast, over the sea (Figures 4a and 4b). Before sunrise, ozone concentration fields show strong ozone titration at ground level due to the presence of NO, in a plume which extends on the coast from Marseille to Fos-Berre and is transported over the sea up to the southeastern end of the domain. After 1000 UTC, the sea breeze develops over the sea with the wind veering to the west/southwest [*Bastin et al.*, 2006] (Figure 4c). The anthropogenic plumes are redirected toward the coast mainly between Fos-Berre and Marseille, and are finally transported back toward the coast and are stretched along a band extending from Fos-Berre to Toulon. This return transport combines with fresh coastal pollutant emissions, amplifying ozone concentrations along the coast (Figures 4b, 4c, and 4d). On that day the ozone concentrations over the whole domain remain moderate (<90 ppb threshold value, corresponding to the first level of public alert) except near Toulon where observed concentrations reach about 100 ppb, values which are underestimated by the simulation. Efficient dispersion due to moderate Mistral and strong mixing leads to low ozone production on that day, despite the limited inland penetration of the sea breeze (about 20–30 km; see Table 1). After 1800 UTC (Figure 4e), whereas ozone concentrations over the sea are still high, ozone is titrated inland in the largest areas with anthropogenic emissions. At night, the wind at ground level becomes weaker with changing direction. It is the time of the onset of the land breeze which brings back pollutants over the sea.

[30] On 25 June, the meteorological situation is mostly influenced by local-scale phenomena. During nighttime (Figure 5a), the wind is weak (land breeze and katabatic winds), and surface ozone concentrations are low due to nighttime titration by NO in the large anthropogenic emission zones and dry deposition. Over the sea, the wind blows from the north/northwest direction on the central part of the domain, whereas it is openly westerly on the area of Toulon, generating a recirculation of the industrial nighttime plumes over the city. This phenomenon can be observed through the trail of an anthropogenic plume (with low ozone concentrations) extending from Fos-Berre to Toulon and spreading up to about 50 km over the sea. After 0900 UTC (Figure 5b), surface ozone concentrations increase. This increase can be related both to the development of the PBL and the recovery of high ozone concentrations in altitude and to local ozone production, as the simulation indicates ozone production rates exceeding 10 ppb h^{-1} downwind the largest anthropogenic areas. At the sea breeze onset, the wind veers to the south/southwest, with a more pronounced westerly component in the region of Toulon [*Bastin et al.*, 2005], which pushes back the primary pollutant plumes toward the coast

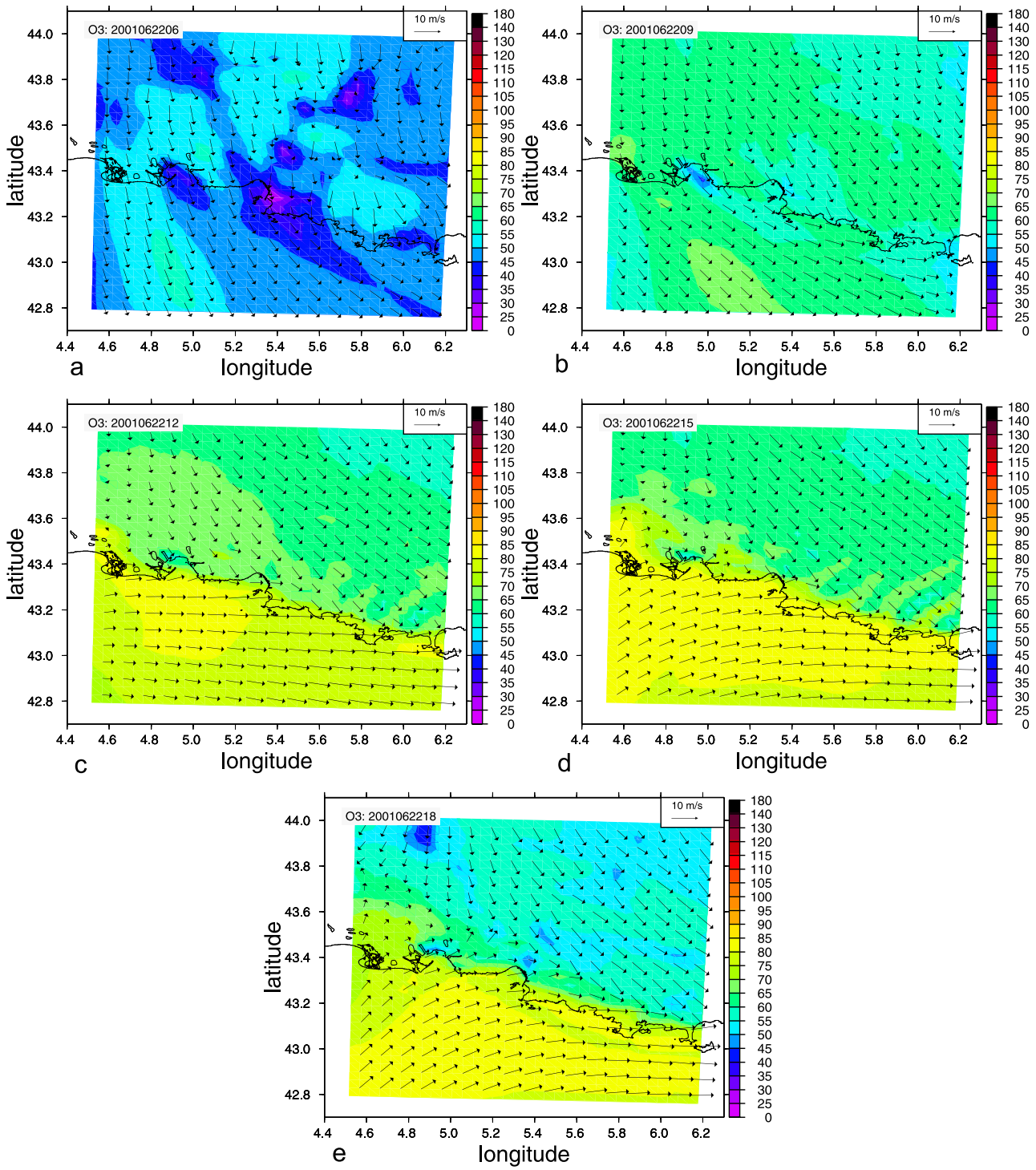

Figure 4. Surface ozone concentration (color coded) and 10 m wind speed and direction (arrows) on 22 June (IOP 2a) at (a) 0600 UTC, (b) 0900 UTC, (c) 1200 UTC, (d) 1500 UTC and (e) 1800 UTC simulated using the MM5 mesoscale model coupled with the chemistry transport model CHIMERE.

where they dilute in a deeper PBL and combine with fresh coastal emissions. Just downwind of Toulon, Marseille and the industrial Fos-Berre complex, fast ozone production is found (from 20 to 35 ppb h^{-1}). After 1100 UTC (Figure 5c), the production rates can reach a maximum of 35 to 50 ppb h^{-1}. Such values, which correspond to the highest range of ozone production rates found in the literature [e.g., *Baumann et al.*, 2000; *Daum et al.*, 2000], are consistent with the experimental calculations made for this period [*Coll et al.*, 2005]. After 1100 UTC, ozone concentration exceeds the threshold value of 90 ppb. Contrary to 22 June, the sea breeze penetrates inland, advects the plume of ozone with values exceeding 90 ppb and forms a band of high concentration extending from Avignon to Toulon. Under

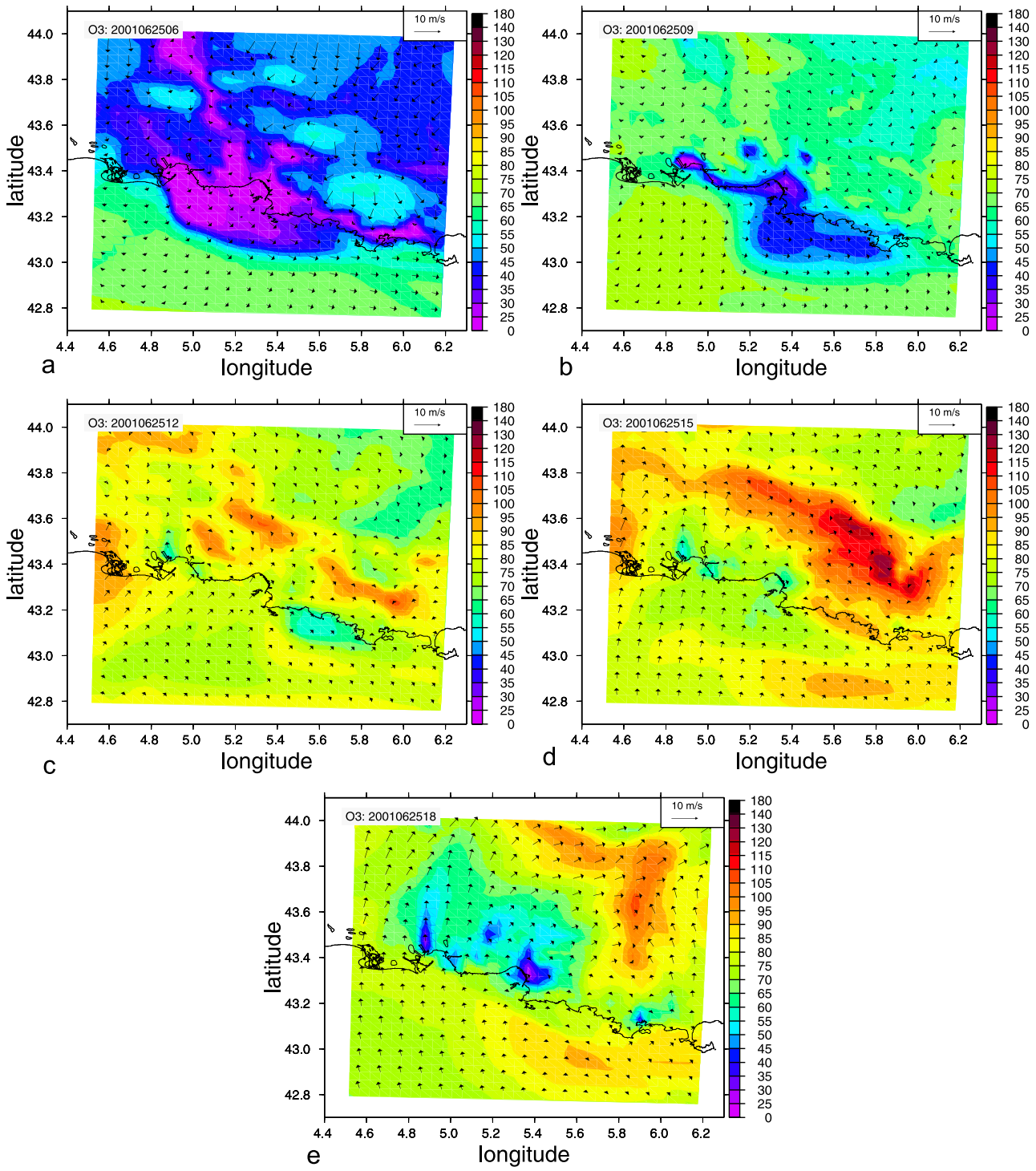

Figure 5. Same as Figure 4 on 25 June (IOP 2b).

the influence of a well-established sea breeze, this high-ozone plume progresses toward the north of the ESCOMPTE domain, its northern end being delimited by the sea breeze front [*Menut et al.*, 2005] (Figures 5d and 5e; it must be noted that in the middle of the Rhône valley, not shown, the sea breeze front penetrates farther inland; see Table 1). Thus most of the ozone is actually produced within the sea breeze which mixes and transports anthropogenic pollutants inland toward the Durance and Rhône valleys. At 1500 UTC (Figure 5d), the local ozone maxima have merged into a single plume which amplitude increases with time and which extreme values, east of Aix en Provence, exceed the 120 ppb threshold at 1600 UTC. On 25 June the simulated ozone concentrations, although a little shifted toward the south compared to measurements, are in good agreement with the maximum of 120 ppb measured at the same time in Cadarache, east of Aix en Provence. After 1500 UTC, ozone production rates fall

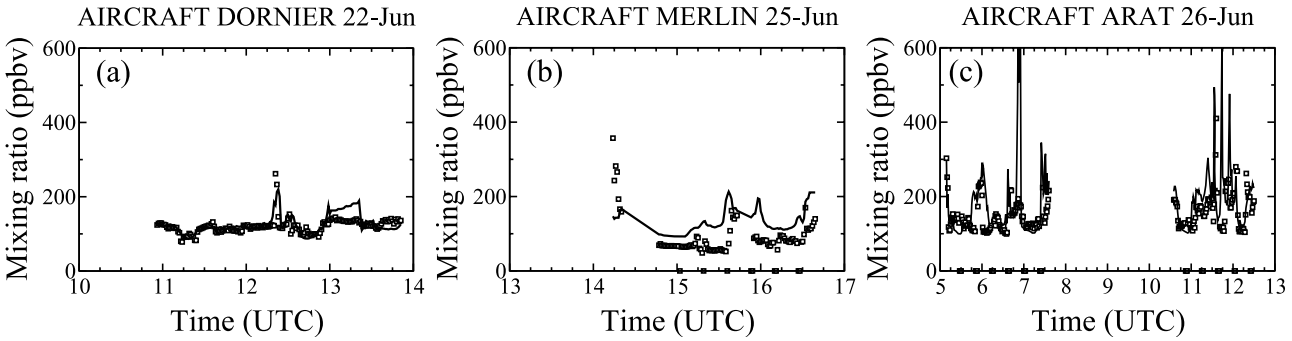

Figure 6. Carbon monoxide concentrations (in ppbv) measured (dots) and simulated by the CHIMERE model (line) onboard the DORNIER, MERLIN, and ARAT aircrafts on 22, 25, and 26 June, respectively. Adapted from *Lasry* [2006].

appreciably, and from 1600 UTC the plume does no longer produce ozone. It is evacuated toward the northeastern part of the domain along the Durance valley. After 1900 UTC (Figure 5e), ozone deposition is simulated downwind the main traffic, urban and industrial centers.

[31] These days are representative of the different types of episodes encountered in the ESCOMPTE region. Days with moderate ozone production are characterized by a sea breeze coupled with moderate synoptic wind like Mistral. Mistral leads to the formation of an ozone plume along the

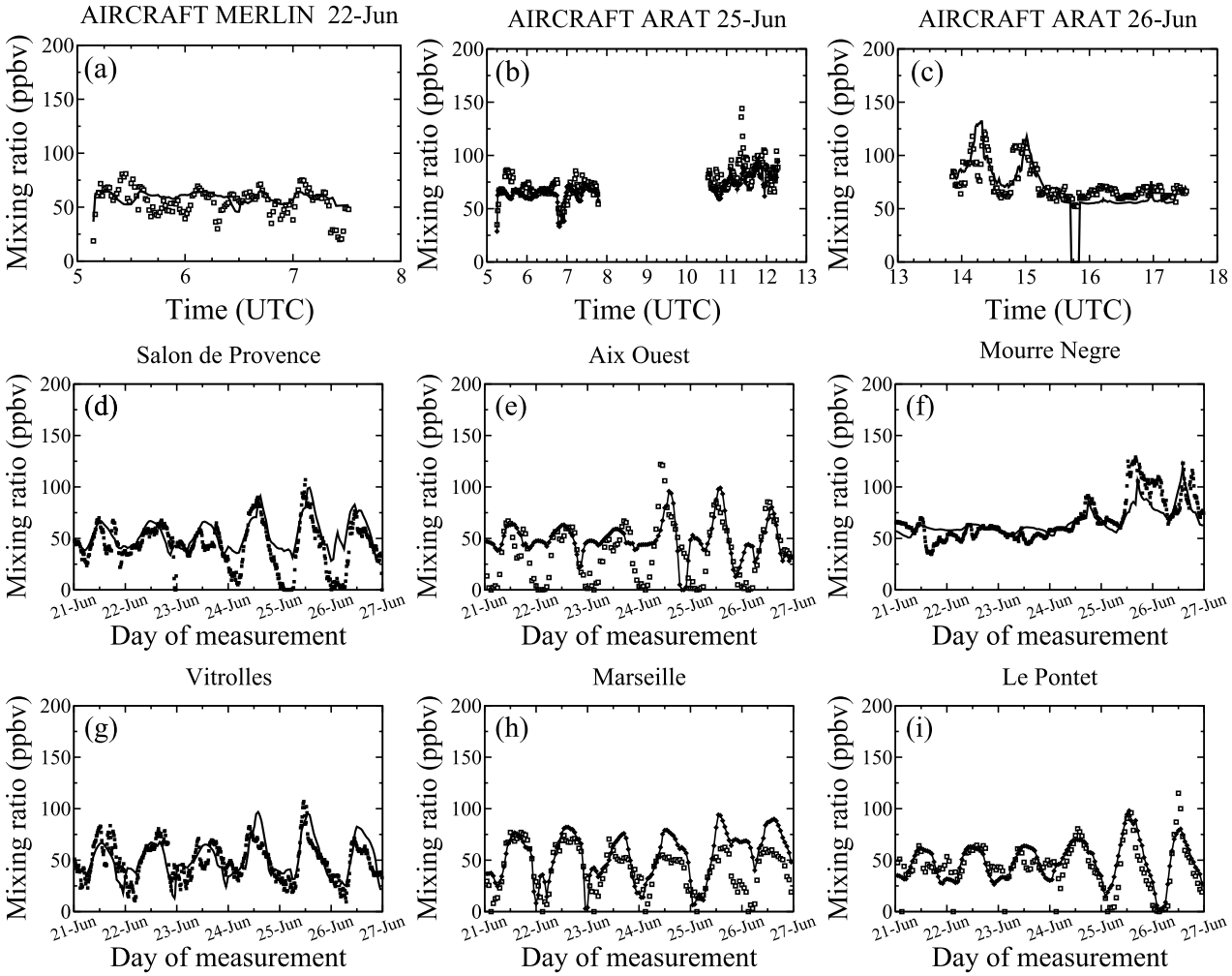

Figure 7. (a–c) Ozone concentrations (in ppbv) measured (dots) and simulated by the CHIMERE model (line) on 22 June onboard the MERLIN aircraft and on 25 and 26 June onboard the ARAT aircraft. (d–i) Ozone concentrations (in ppbv) measured (dots) and simulated by the CHIMERE model (line) for 6 ground stations (see Figure 1) between 21 and 27 June (IOP2). Adapted from *Lasry* [2006].

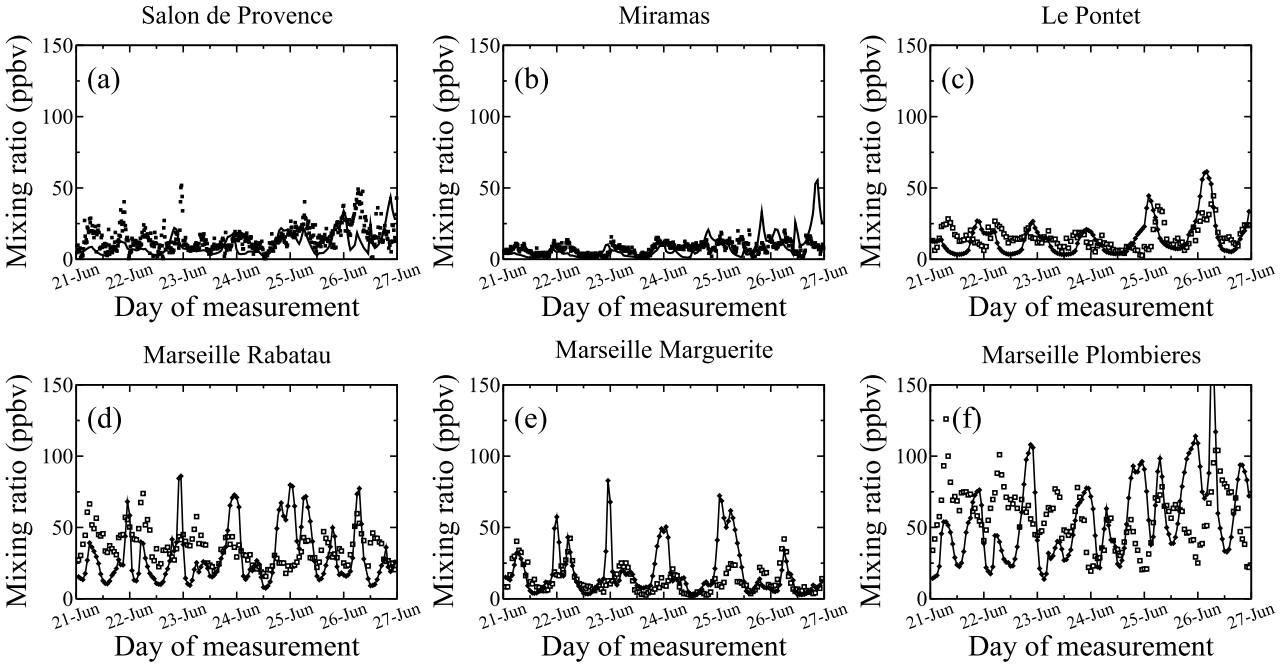

Figure 8. Nitrogen dioxide concentrations (in ppbv) measured (dots) and simulated by the CHIMERE model (line) for 6 ground stations (see Figure 1) between 21 and 27 June (IOP2). Adapted from *Lasry* [2006].

coast close to Toulon (14 June, i.e., IOP1 and 21–23 June, i.e., IOP2a) with concentrations slightly exceeding 90 ppb. The numerical prediction of the exact timing and location of the advected ozone plume in coupled Mistral/breeze situations is made complex by the strong sensitivity of the convergence zone location to the balance between sea breeze and large-scale wind (Table 1). Location and timing of the ozone plumes are also sensitive to topographic details which may be difficult to represent in models. The ozone plumes observed in Toulon are particularly difficult to simulate [*Cousin et al.*, 2005]. The situation of 24 and 25 June are representative of these types of meteorological situations. Maximum ozone concentrations are mainly recorded between 10 km and 50 km downwind the main anthropogenic sources (25 June, i.e., IOP2b, and Ju03, i.e., IOP3), the plume being often evacuated in the Durance valley and along the mountain slopes even though on some occasions the plume may also penetrate less far inland because of adverse synoptic wind (24 June and 10 July, i.e., IOP4). Despite slight deviations in the wind direction that make difficult the restitution of the exact location of the peaks, the main characteristics of these episodes are fairly well numerically reproduced with a day-to-day variability of the peak intensity that is also in good agreement with measurements. All these ESCOMPTE days have been simulated using various dynamical and chemistry transport models and *Dufour et al.* [2005] and *Taghavi et al.* [2005] show that not surprisingly, modelled photochemistry within the PBL is quite sensitive to refinements in the emissions, particularly primary compounds, as well as to the chemical scheme employed.

4.2.2. Impact of the Rhône and Durance Valleys on Mesoscale Transport

[32] The impact of the Rhône and Durance valleys on the sea breeze dynamics (depth, intensity and penetration) has been investigated by *Bastin et al.* [2005] and *Drobinski et al.* [2006]. They show that the sea breeze is generally affected by flow splitting between the Durance and the Rhône valley whenever it reaches the bifurcation zone (it is not the case during IOP2a). If the sea breeze flow reaches the entrance of the Durance valley (other IOPs), it is then accelerated in the Durance valley due to lateral constriction and progresses farther inland. In presence of an offshore flow in the Rhône valley (21–25 June and 10 July), lateral constriction does not affect the sea breeze. On 26 June and 3 and 4 July, the combination with an onshore flow leads to farther penetration inland and intensification of the low-level southerly flow in the Durance but also in the Rhône valley. If the onshore synoptic flow is too strong, the sea breeze flow can be inhibited as on 4 July in a large area in the Rhône valley [*Drobinski et al.*, 2006]. The impact of valley channeling on ozone plume penetration has been investigated quantitatively for IOP2b. Time series of ozone concentration at different ground stations along the Durance and Rhône valleys indicate clearly the distinction between the peak of photochemistry at 1200 UTC, and the peak due to ozone production associated with sea breeze transport around 1500–1800 UTC (Table 2). Between 1500 and 1800 UTC, photochemistry production decreases to about 25% of the maximum found at 1200 UTC. The observed ozone increase between 1200 and about 1800 UTC, at a rate of about 7–10 ppb h^{-1} (with a maximum of 40 ppb h^{-1}), is thus mainly due to transport. In the Rhône valley, wider than the Durance valley, the plume of ozone precursors is more diffuse and the ozone peaks are generally lower.

4.3. Vertical Transport and Mixing

[33] Section 4.1 shows that large-scale atmospheric circulation is a major cause of ozone distribution in the free troposphere in the ESCOMPTE target area. One key ques-

Table 2. Ozone Concentration at Different Ground Stations Located Along the Rhône and Durance Valleys at About 1200 UTC and Between 1500 and 1800 UTC (Maximum Ozone Value)[a]

	Distance From the Coast	24 Jun	25 Jun	26 Jun
Alpilles (Rhône valley)	35 km	72.3/85.4	100.2/111.7	80.5/57.5
Le Pontet (Rhône valley)	50 km	65.7/78.9	78.9/94.0	85.4/111.7
Bollène (Rhône valley)	90 km	63.4/71.6	75.1/78.6	65.7/91.5
Meyrargues (Durance valley)	45 km	79.3/114.1	96.7/106.4	81.2/98.6
Vinon (Durance valley)	60 km	55.8/91.7	71.9/124.0	62.6/119.7
Les Mees (Durance valley)	80 km	57.3/87.8	72.5/135.9	71.0/109.2

[a]Left number is 1200 UTC, and right number is between 1500 and 1800 UTC. Values are in ppb.

tion is the estimation of the air mass exchanges between the PBL and the free troposphere which can contribute to ventilate the PBL or to import fresh ozone from the free troposphere down to the PBL, enhancing the contribution of local emission sources. In the ESCOMPTE region, the dynamical processes that contribute to vertical exchanges and mixing consist of (1) the vertical mixing at the sea breeze front, (2) the entrainement/detrainement processes at the convective PBL top in the following sea breeze, and (3) the contribution of the slopes to venting/accumulation processes by anabatic/katabatic flows.

4.3.1. Vertical Mixing at the Sea Breeze Front

[34] The leading edge of the sea breeze forms in general a typical frontal zone with intense turbulence mixing while a sharp dividing line is maintained between the sea breeze flow and the environmental flow. Figure 9 shows the passage of the sea breeze front above the UHF wind profiler

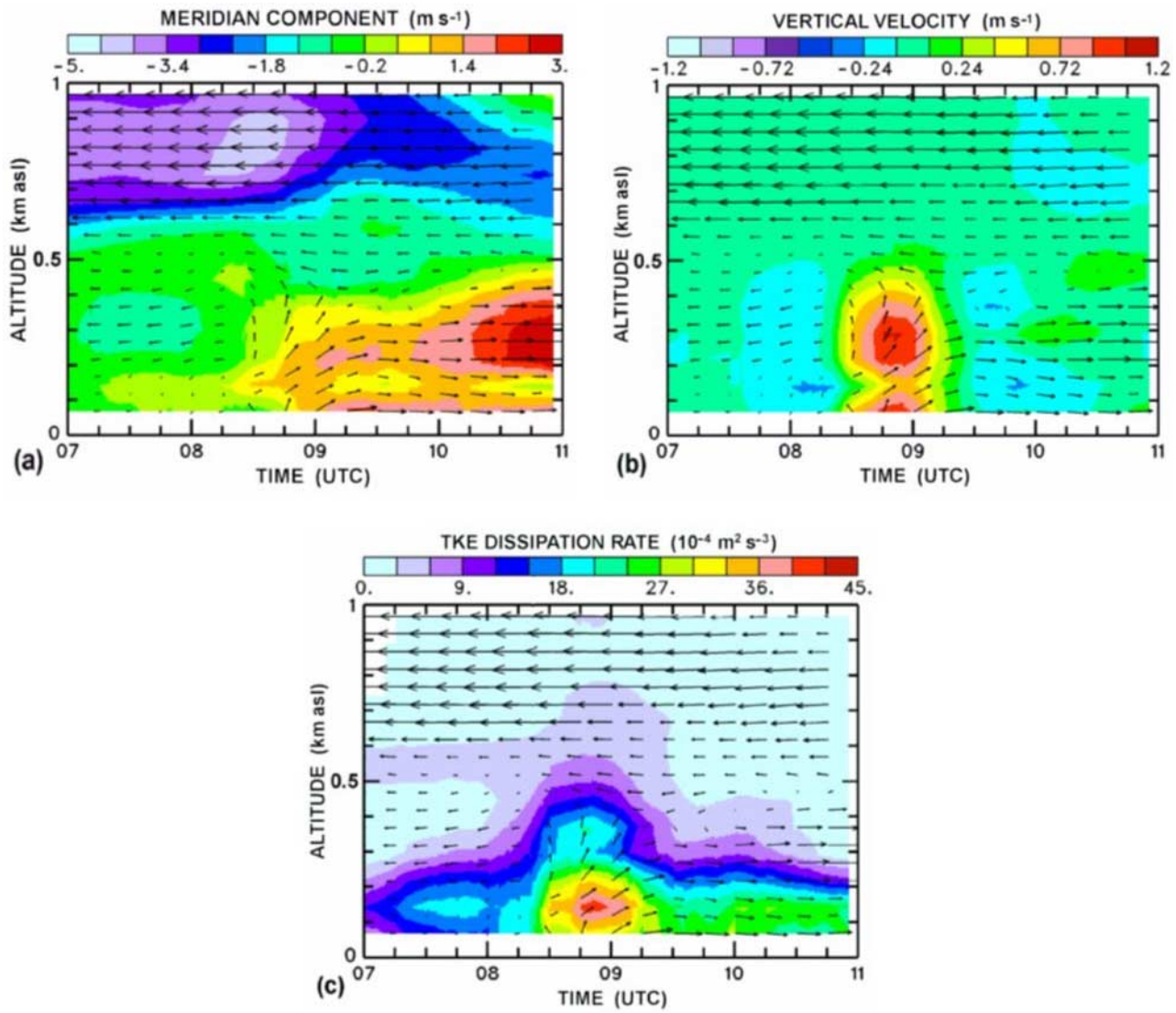

Figure 9. Time-height sections of meridian wind speed (i.e., the south-north wind component v), vertical wind components, and dissipation rate measured with Saint Chamas UHF wind profiler on 24 June, with superimposed (v, w) wind vectors. Adapted from *Puygrenier* [2006].

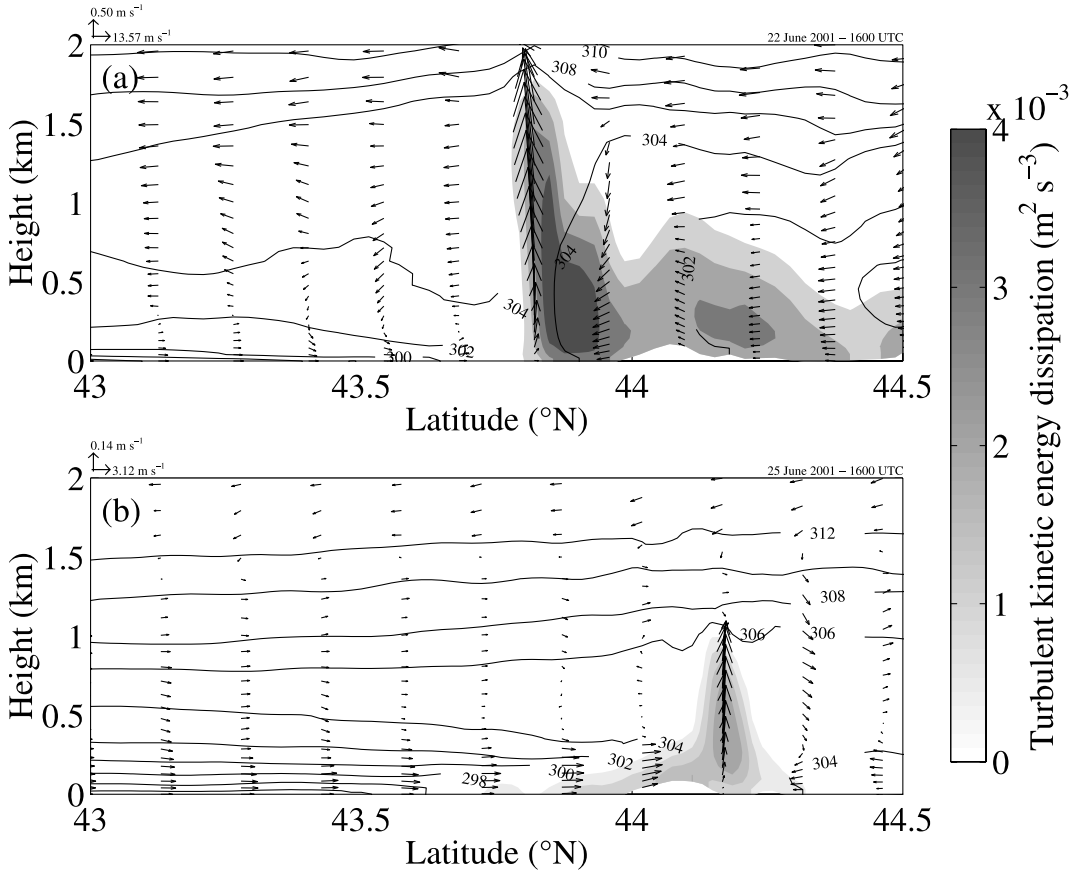

Figure 10. Vertical cross section at 4.5°E longitude of $v - w$ wind vectors (arrows, with v the meridian wind component and w the vertical wind component), potential temperature (isocontours ranging from 294 K to 310 K with a 2 K interval), and turbulent kinetic energy dissipation rate (shaded area) at 1600 UTC on (a) 22 June 2001 and (b) 25 June 2001 along the Rhône valley, as simulated by the Méso-NH model. The vertical and horizontal arrows indicate the scale for w and v, respectively. Adapted from *Bastin and Drobinski* [2006] and *Bastin et al.* [2006].

on 24 June (IOP2b) at Saint Chamas [*Puygrenier*, 2006]. This unique data set perfectly illustrates the dynamics of the sea breeze front. The sea breeze starts blowing at Saint Chamas (very close to the shore) at about 0900 UTC when the wind takes a southerly component. The passage of the sea breeze is materialized by strong updraft (>1 m s^{-1}) and large dissipation rate (about 45 $\times$ 10^{-4} m^2 s^{-3} maximum) up to about 0.5 km. Maximum turbulence is found up to about 0.3 km within the sea breeze head due to large gradient of horizontal wind speed through the sea breeze front generating shear induced turbulence. After the passage of the front, the sea breeze is only 0.3 km deep with still large dissipation rate (about 30 $\times$ 10^{-4} m^2 s^{-3} maximum) due to near-surface shear and buoyancy production of turbulence by convection. One can note the weak downward motion following the passage of the sea breeze front associated with detrainment in the wake of the sea breeze front. The UHF observations can be compared qualitatively to the numerical simulations by *Bastin et al.* [2006] and *Bastin and Drobinski* [2006] for 22 June and 25 June, respectively. Figure 10 shows a vertical cross section of $v - w$ wind vectors (v is the meridian wind component), dissipation and potential temperature at 1600 UTC along the Rhône valley (4.5°E longitude) on 22 June (IOP2a) and 25 June (IOP2b) as simulated with the Méso-NH model. It clearly evidences a maximum updraft (0.5–1 m s^{-1}) and a sea breeze "head" extending up to about 1 to 2 km asl. *Bastin et al.* [2006] show that the speed of the sea breeze flow (about 5 m s^{-1}) is faster than the speed of the see breeze front (about 1–2 m s^{-1}), so when the sea breeze flow reaches the front, convergence results in a rapid updraft flow and a characteristic "head" forms at the sea breeze front, typical of a gravity current and deeper than the following sea breeze flow. This raised head is a zone of intense mixing as indicated by the large values of dissipation rate. One can note that the simulated values of vertical velocity and dissipation rate are of the same order than those measured by the UHF wind profiler (Figure 9).

[35] *Bastin and Drobinski* [2006] computed mass flux at the sea breeze front. They show that the vertical mass fluxes can take values half as large as the sea breeze induced horizontal air mass flux in the Rhône valley. Detrainment in the wake of the sea breeze front does not compensate for this net upward export of air mass from the PBL to the free troposphere. This is visible in Figures 9 and 10 with upward motion penetrating deeply in the free troposphere. *Bastin*

and Drobinski [2006] conclude that the most efficient transport from the PBL to the free troposphere is found at the sea breeze front especially in situations of moderate offshore synoptic flow. Since the sea breeze front propagation speed is lower than the sea breeze intensity, and because the vertical mass flux at the front is smaller than the horizontal mass flux in the sea breeze, the pollutants accumulate just behind the front (Figures 4 and 5), part of them being exported upward at the sea breeze front [*Cousin et al.*, 2005]. This is illustrated in Figure 11, which shows the three-dimensional structure of the ozone field along a south-north cross section intersecting the coast line near Marseille, characterized by a typical pattern where the ozone maximum is found along the sea breeze front, transported and lifted at upper levels in the convergence line. Figure 11 shows the progression of the ''ozone front'': in the late morning the plume develops near the coast in a weakly polluted background air, is farther advected inland, lifted and recirculated by both the weak Mistral and the upper sea breeze branch. At the end of the afternoon this coupling between mesoscale transport and photochemistry leaves an ozone layer that fills the residual layer as also suggested by *Millán et al.* [1996] from the MECAPIP data. This phenomenon can be substantially attenuated in the morning and in the evening (at the onset and breakdown of the sea breeze when the front is smooth, see Figures 11a and 11e) and in situations of onshore synoptic prevailing wind [*Estoque*, 1962]. The tropospheric rich-ozone air masses documented by the ozone lidars at Aix les Milles (Figure 2) and originating from the PBL have thus most probably been lifted above the PBL at the passage of the sea breeze front that has transported upward the polluted air of the Marseille and Fos-Berre plumes (see section 4.1).

[36] More locally, in the Marseille area which displays a step like coastline, a shallow sea breeze (about 300 m depth) driven by the local coastal temperature gradient, blows perpendicular to the coastline below the main southerly sea breeze, forced by the regional temperature contrast between land and the Mediterranean sea (also called deep sea breeze). Because of the shape of the Marseille coastline (the city faces the sea both to the east and to the south), the shallow sea breeze blows from the south-southeast south of Marseille, and from the west over the northern districts [*Bastin and Drobinski*, 2006; *Lemonsu et al.*, 2006a]. *Lemonsu et al.* [2006a] show that the southerly shallow sea breeze south of Marseille and the westerly shallow sea breeze north of Marseille converge and form a marked front over the city center forcing updrafts which export urban ozone at higher vertical levels as discussed by *Delbarre et al.* [2005]. Frontogenesis associated with the sea breeze (both shallow and deep) thus appears to be a very efficient way to export pollutants from the surface to the upper levels.

4.3.2. Turbulent Vertical Transport in the PBL

[37] During ESCOMPTE, the impact of convective motions within the PBL on vertical exchanges of temperature, humidity, ozone and nitric oxides has been quantified [*Kalthoff et al.*, 2005] because entrainment and detrainment at the PBL top may contribute to downward mixing of air pollutants from elevated layers into the PBL, increase surface concentrations and initiate chemical transformation processes. Because NO and NO_2 sources reside near the Earth's surface, nitrogen oxides deviate positively in the convective updrafts throughout the PBL and therefore the turbulent flux of NO_x, $\overline{w'NO_x'}$ (where w' and NO_x' are the turbulent fluctuations of the vertical velocity and NO_x concentration, respectively) is positive in general both over the Rhône valley and the mountainous terrain (Figure 12). However, the flux data over the mountainous terrain show a much higher variability and sometimes are even twice as high as over the Rhône valley. This may be attributed to local sources and secondary circulations, such as anabatic slope winds.

[38] In contrast to nitric oxides, ozone is both produced locally by photochemical reactions involving anthropogenic produced precursors and transported into the region over quite long distances [e.g., *Corsmeier et al.*, 2005]. The relation between ozone production and destruction depends on the concentration of precursor gases, radiation, humidity and temperature [*Klonecki and Levy*, 1997]. Transport of stratospheric ozone into the troposphere takes place too [*Colette et al.*, 2006], but is not a major factor [*Hasel et al.*, 2005]. Figure 12 shows that the vertical ozone fluxes in the PBL over the Rhône valley are slightly negative with values of about 0.15 ppb m s^{-1}. Ozone is transported toward the surface where deposition takes place. Much more variability occurs over the mountainous areas, $\overline{w'O_3'}$ (where O_3' is the turbulent fluctuation of O_3 concentration) varying between ± 0.5 ppb m s^{-1} with a mean value of about zero. The highest values of $\overline{w'O_3'}$ occur at the PBL top, with in average negative sign over the mountainous sites and positive over the Rhône valley. However, high variability at the PBL top indicates entrainment and detrainment processes with the free atmosphere. The negative covariance over the mountains results from the ozone profile, which shows a maximum at the PBL top due to ozone transport along the mountain slopes (except on 26 June, not shown, when the PBL is highly polluted, resulting in a significant ozone gradient toward lower concentrations in the free troposphere during daytime associated with positive covariance and an effective transport of ozone from the PBL to the free troposphere). This downward flux over the mountains associated with detrainment at the leading edge of the upslope winds validates qualitatively the numerical results of *Bastin and Drobinski* [2006] for 25 June and is consistent with the experimental and numerical findings by *Saïd et al.* [2007]. However, the mass flux budget by *Bastin and Drobinski* [2006] also shows that this detrainment within the PBL does not compensate the vertical export in the free troposphere by the combination of upslope winds and the sea breeze.

[39] It has thus been shown during ESCOMPTE that ozone transport is mainly directed toward the sink region at the earth and vegetation surfaces. Since O_3 is controlled by radiation, concentration of precursors and temperature, the ozone concentration in the PBL is characterized by a high variability in cases of high air pollution. In mountainous regions, fluxes are mainly negative. Entrainment and detrainment at the PBL top may critically affect exchange with the free troposphere.

4.3.3. Vertical Venting Along the Slopes

[40] Finally, the ESCOMPTE target area is featured by many massifs surrounding the city of Marseille and in the countryside and the foothills of the western Alps. The

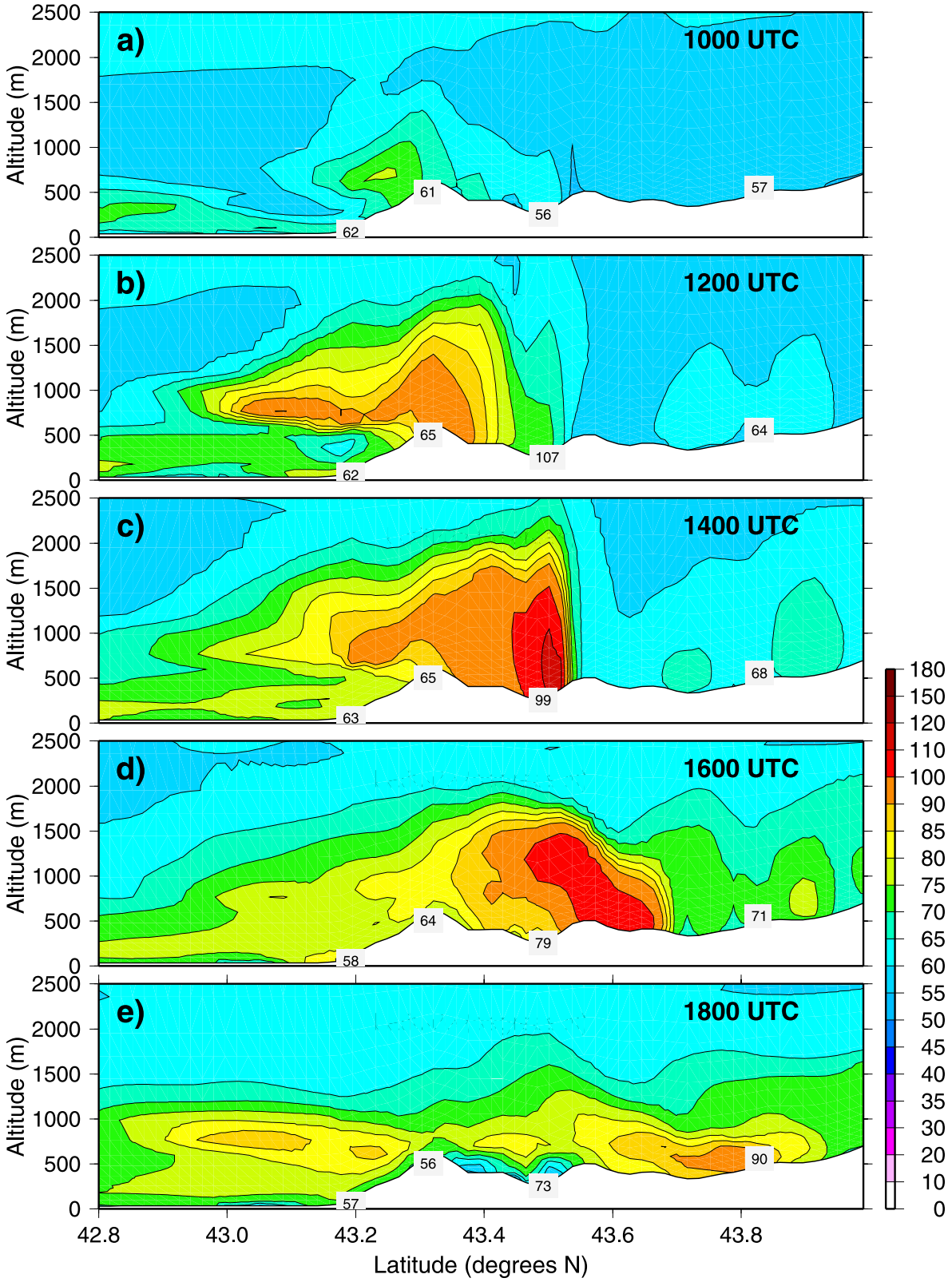

Figure 11. South-north cross section the ozone concentration field (ppb) simulated by the CHIMERE chemistry transport model on 24 June. The cross section is taken at 5.65°E. In this simulation the model is run at a resolution of 2 km, has 16 layers between ground level and 500 hPa, and is driven by the MM5 model, itself forced at the boundaries by the ECMWF analyzes. The model topography is represented. Abscissa represents the latitude.

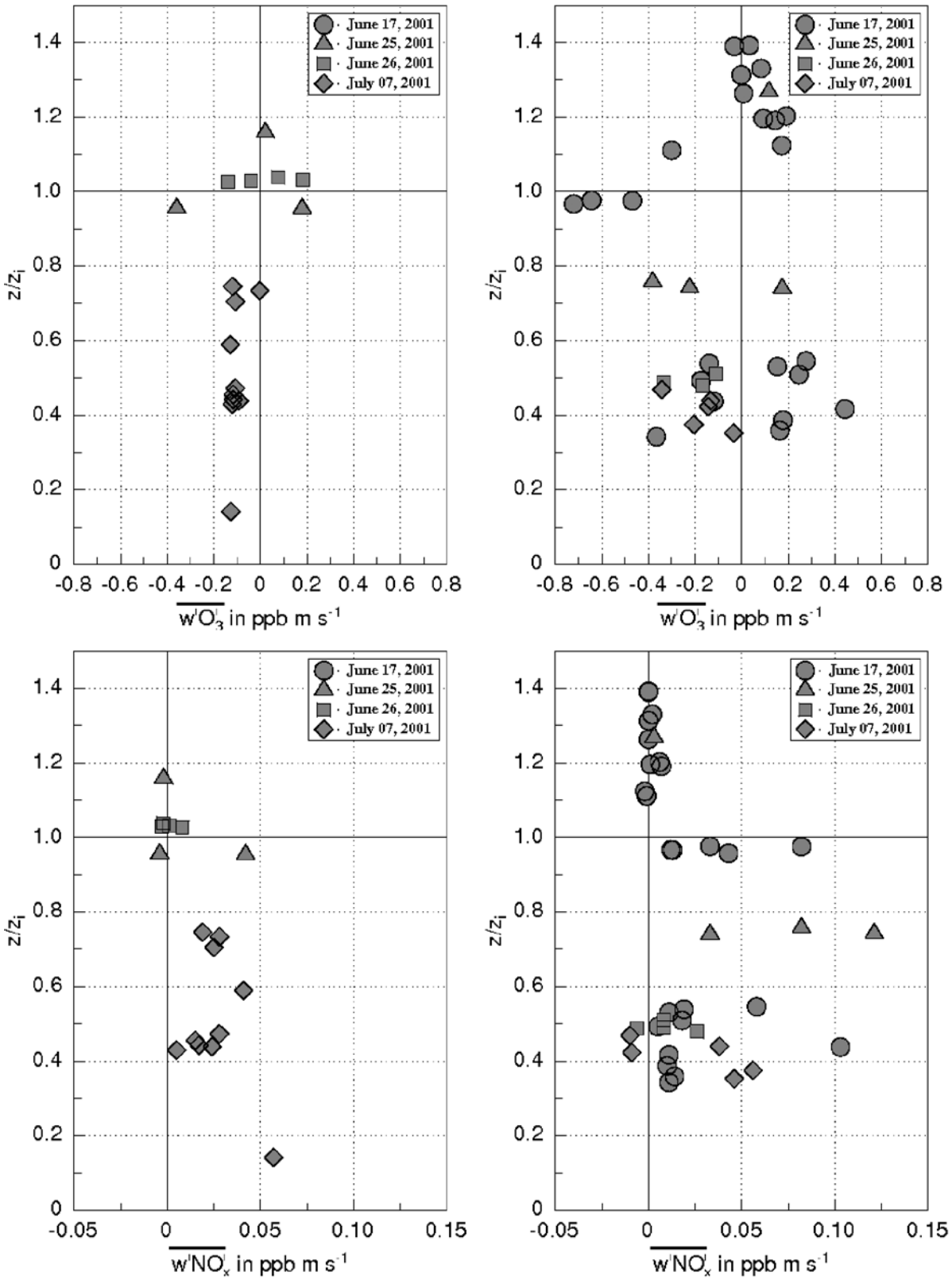

Figure 12. Vertical profiles of turbulent ozone fluxes and nitric oxide fluxes (left) over the Rhône valley and (right) over the mountain ranges. Adapted from *Kalthoff et al.* [2005].

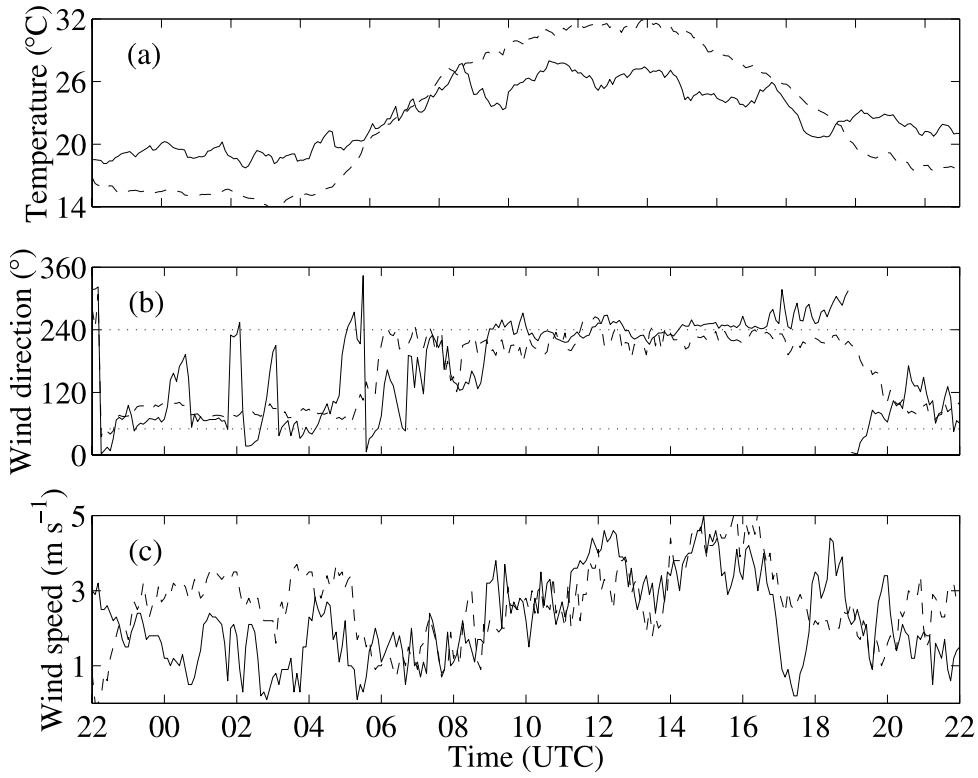

Figure 13. (a) Time evolution of 2 m surface temperature, (b) 10 m wind direction, and (c) speed at Vallon d'Ol (solid line) and Barben (dashed line) (see Figure 1) on 25 June. The dotted lines in Figure 13b indicate the upslope (240°) and downslope (50°) directions. Adapted from *Bastin and Drobinski* [2005], with kind permission of Springer Science and Business Media.

orography affects the low-level atmospheric circulation as an obstacle but also can generate slope winds that contribute to pollution venting during daytime by anabatic upslope flows and by pollution accumulation during nighttime by the katabatic winds. Using numerical simulations, *Bastin and Drobinski* [2006] showed that slope wind contribute to export air mass from the PBL into the troposphere. The combination of the sea breeze with the slope wind tend to increase the vertical mass flux along the slope by at least a factor of two. From an observational point of view, the dense observation network near Marseille allowed the documentation of the slope winds and their impact on ozone distribution. The works conducted by *Bastin and Drobinski* [2005] and *Puygrenier et al.* [2005] show that land and sea breezes flowing along the nearshore sloped terrain oscillate with time with a period of 45 to 90 min during nighttime, and 2 to 3 hours during daytime. These oscillations are visible in surface temperature and wind velocity, PBL depth but also in ozone and nitrogen oxide. The most striking example is on 25 June. Figure 13 displays the time series of measurements of temperature, wind direction and speed by the surface station at Vallon d'Ol, north of Marseille on a hill flank with a gentle slope of 3°. Figure 13 shows a 180° rotation of the wind direction between 0600 and 0900 UTC (from the northeast to the southwest) and at 1900 UTC (from the southwest to the northeast) associated with the sea breeze and land breeze onsets. During nighttime (2200–0600 UTC), the wind is very weak (about 1 m s^{-1}) with a mean direction of about 70° (northeast direction). Figure 14 shows a nighttime temperature oscillations with a period of about 1 and a 1.5 hour modulation. The northeast component of the oscillating katabatic flow indicates that the air drains off the mountain along the maximum slope direction at Vallon d'Ol. During daytime, the wind direction is about 250°, corresponding to the sea breeze and maximum slope directions at Vallon d'Ol. Figures 13 and 14 reveal the existence of daytime oscillations in temperature and velocity with a period of nearly 3 hours. *Puygrenier et al.* [2005] showed that the oscillation of the wind speed is visible up to the PBL top which also oscillates with an amplitude of about 200 m. Figure 13 shows that at Barben (30 km northwest of Vallon d'Ol) on a flat terrain area affected by land and sea breezes, no oscillation is visible during both nighttime and daytime. For katabatic winds, *Fleagle* [1950, p. 230] explains the oscillating phenomenon simply: "as the air accelerates down the slope, adiabatic heating results in a reverse pressure gradient which retards the flow. As the air decelerates, friction decreases, radiative cooling increases the pressure gradient and the cycle is repeated." Comparatively to katabatic winds, no daytime observations of oscillating anabatic upslope flows have ever been published, probably because of temperature inversion breakup that inhibits upslope winds [*Whiteman and McKee*, 1982a, 1982b]. During ESCOMPTE, the existence of such oscillation is attributed by *Bastin and Drobinski* [2005] to the sea breeze which advects cold air and thus imposes a mesoscale temperature gradient that forces the baroclinicity of the

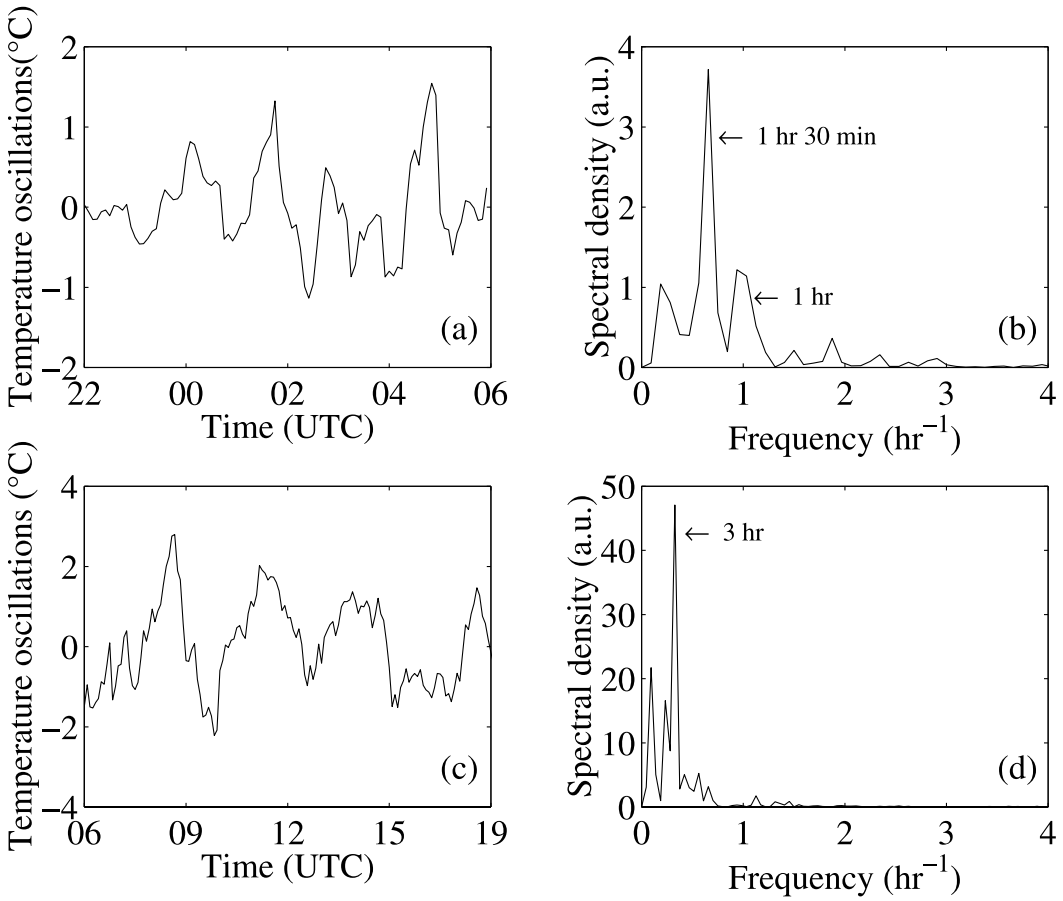

Figure 14. (a) Time series of the temperature oscillations on the night of 25 June at Vallon d'Ol between 2200 and 0600 UTC (b) with its corresponding power spectrum (obtained using a Bayesian spectral estimator). (c and d) Same as Figures 14a and 14b except for the time series between 0600 and 1900 UTC. Adapted from *Bastin and Drobinski* [2005], with kind permission of Springer Science and Business Media.

atmosphere all day long. The mechanism of the observed oscillations is thus very similar to low-frequency oscillations of katabatic flows: (1) the isentrope inclination allows the sea breeze flow to run along the slope; (2) the adiabatic cooling due to the air ascension retards the flow; (3) the radiative heating near the surface allows the flow to accelerate.

[41] By simplifying and combining the equations of motion and heat, *Bastin and Drobinski* [2005] derived a differential equation which describes a harmonic oscillation of wind and temperature with the following pulsation frequency:

$$\omega = \sqrt{\frac{g}{\theta_0}\sin\alpha\left(\frac{\partial\left(\bar{\theta}+\theta^{\star}\right)}{\partial x}\cos\alpha + \Gamma\sin\alpha\right)} \qquad (1)$$

where g is the gravity acceleration, θ_0 is a reference potential temperature, $\bar{\theta}(x, z, t)$ the mesoscale potential temperature field, $\theta^{\star}(x, z, t)$ is the perturbation with regards to the mesoscale field due to the existence of the gravity flow. $\partial\bar{\theta}/\partial x$ is the horizontal gradient of potential temperature due to the existence of the sea breeze flow, $\Gamma = \partial\theta/\partial z$ is the vertical lapse rate of the atmosphere, and α is the slope angle. Table 3 gives additional details about the date, the average wind direction as well as the observed and predicted oscillation period for the nights and days showing evidence of temperature and velocity oscillations.The oscillation time period varies between 45 and 90 min at night whereas during daytime it varies between 100 and 180 min.

[42] The agreement between the observed nighttime oscillation periods and the predictions using equation (1) was found for the whole campaign (Table 3). The absence of wind and temperature oscillations during IOP 2a along the slope surrounding the city of Marseille is mainly due to the fact that the sea breeze hardly reached the sloped terrain region as shown by *Bastin et al.* [2006].

[43] The impact of such oscillations on ozone concentration is discussed by *Puygrenier et al.* [2005] and *Augustin et al.* [2006]. Figure 15 displays NO_2 and O_3 concentrations measured in the Marseille city center between 0900 and 1900 UTC. Figure 15 shows that NO_2 concentration falls periodically from 30–35 to 15–20 ppb simultaneously with the maxima of the sea breeze intensity (indicated with the black arrows) at 1215–1230, 1400–1500, and 1800–1830 UTC (see Figure 13), whereas O_3 concentration is nearly constant (30–40 ppb) during the day and also falls periodically to 20–25 ppb observed simultaneously with NO_2 concentration maxima. *Puygrenier et al.* [2005] showed that during sea breeze, advected marine air is poor in NO_2

Table 3. Nighttime and Daytime (shaded) Oscillation Periods When the Surface Measurements at Vallon d'Ol Show Evidence of Temperature and Wind Speed Oscillations on June and July 2001[a]

Date (2001)	Wind		Oscillation Period obs./Equation (1)
	Direction	Speed	
7 Jun	W/SW	6 m s^{-1}	100 min/-
7–8 Jun	E	2 m s^{-1}	60 min/-
11–12Jun	E	4 m s^{-1}	70–90 min/-
13 Jun	SW	6 m s^{-1}	180 min/-
14–15 Jun	E	2 m s^{-1}	70 min/80 min
15–16 Jun	E	3–4 m s^{-1}	60 min/75 min
19–20 Jun	NE	2 m s^{-1}	60 min/70 min
20 Jun	SW	5 m s^{-1}	120–140 min/
23 Jun	W/SW	5 m s^{-1}	180 min/170 min
24–25 Jun	NE	1 m s^{-1}	60 min/70 min
25 Jun	W/SW	4 m s^{-1}	180 min/170 min
25–26 Jun	E	2 m s^{-1}	80 min/90 min
26 Jun	W/SW	4 m s^{-1}	120 min/140 min
26–27 Jun	NE	2 m s^{-1}	50 min/70 min
29–30 Jun	N	4–5 m s^{-1}	90 min/90 min
7–8 Jul	N/NW	4 m s^{-1}	60 min/-
8 Jul	SW	7 m s^{-1}	120 min/-
9–10 Jul	NE	2 m s^{-1}	45 min/-
13 Jul	SW	5 m s^{-1}	150 min/-

[a]Daytime periods are indicated in bold. Comparison is made with theoretical prediction given by equation (1) (except from 7 to 13 June and for July 2001 when no vertical profiles of virtual potential temperature were measured). The abbreviation obs. stands for "observations."

and that the NO_2 concentration of the marine air increases as it travels over Marseille. The enrichment in NO_2 increases with the residential time of the marine air over the city. The reason why NO_2 and O_3 concentrations oscillate with the wind speed is the following: (1) when the wind speed is weak and the PBL deep, the concentration of NO_2 increases over Marseille whereas the concentration of O_3 remains low because of dilution; (2) when the wind speed increases, the concentration of NO_2 decreases because the residential time over the city decreases and the concentration of O_3 increases because the PBL depth decreases. However, the competition between three processes (ozone production along the air mass trajectory, residential time over the urban area and PBL depth) can differ from one site to the other in some areas in Marseille [*Augustin et al.*, 2006]. For instance, air mass trajectory, and so ozone loading, differ when the area is on the path of the southerly shallow sea breeze (south of Marseille) or of the westerly shallow sea breeze (north of Marseille) (see section 4.3.1) inducing different correlation between ozone concentration and PBL depth.

[44] So the combination of slope winds with the sea breeze enhances the vertical export along the slopes by about a factor of two with respect to the action of slope winds only. The combination of slope winds with the sea breeze generate oscillating motions along the slopes similar to gravity waves. The oscillating motions is associated with periodic variation of pollutants concentrations due to the modulation of the residential time over the emission sources and by dilution caused by PBL depth oscillation. Venting along the slope thus appears to be a non negligible process in the ESCOMPTE target area.

4.4. Advances in Physical and Chemical Numerical Modeling During ESCOMPTE

[45] One major objective of ESCOMPTE was to improve the performance of high-resolution numerical weather prediction, chemical and coupled models in a complex coastal area. Some limits appeared with respect to the representation of the town energy budget and its impact on the simulated low-level thermodynamical field over Marseille mainly, and grid resolution (since a grid size of a few kilometers is not fine enough to reproduce the fine complex terrain in the region of Marseille and orography of the Rhône and Durance valleys). Most of these problems could be solved using the ESCOMPTE data set, allowing more accurate and reliable numerical modeling and forecasting of the three-dimensional structure of sea breeze and its time evolution, and of the ozone and nitric oxide concentrations.

4.4.1. Town Energy Budget Scheme

[46] In the ESCOMPTE region, the reliable and accurate modeling of the atmospheric in the vicinity and over a large city such as Marseille requires an improved parametrization of energy exchanges between the town and the atmosphere. Numerical simulations performed by *Lemonsu et al.* [2006b] with the Méso-NH model and the town energy budget (TEB) scheme [*Masson*, 2000] for IOP2a and IOP2b demonstrate that a proper treatment of the town energy budget is of crucial importance to simulate accurate surface heat fluxes and temperature in the urban area. Beforehand, the ESCOMPTE database allowed to improve the initial

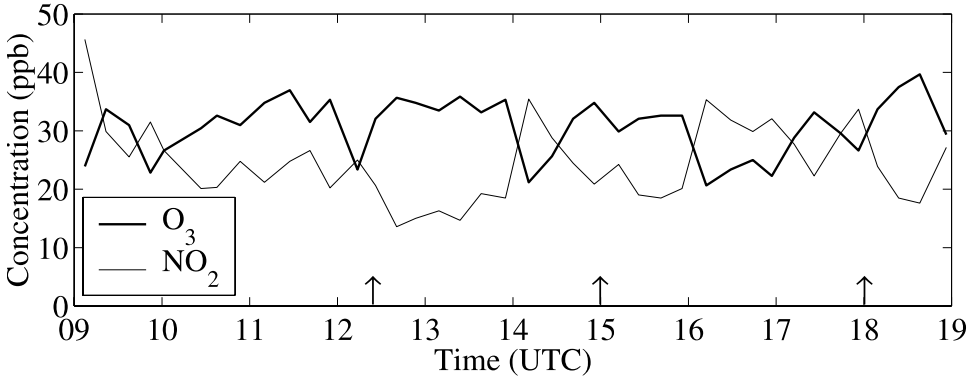

Figure 15. Nitrogen dioxide (NO_2) and ozone (O_3) concentrations measured on 25 June in the Marseille city center (arrows indicate westerly wind maxima). Adapted from *Puygrenier et al.* [2005], copyright 2005, with permission from Elsevier.

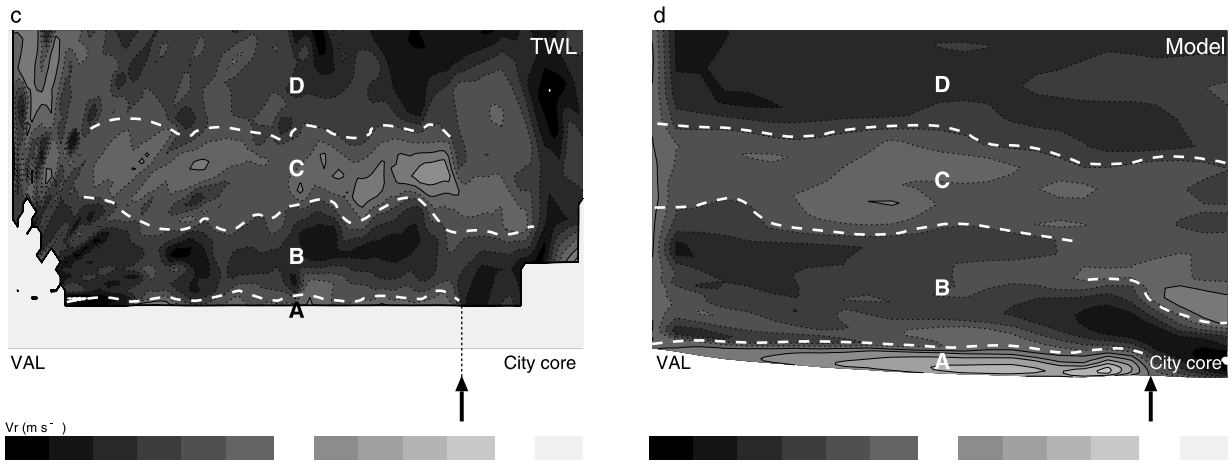

Figure 16. Vertical cross sections of (left) observed (right) and modeled radial velocities along the ground-based Doppler lidar line of sight on 26 June 2001 at 1400 UTC. The solid and the dashed isolines distinguish the positive and the negative radial velocities, respectively. The model outputs correspond to the 250 m domain grid size, which is similar to the radial resolution of the ground-based Doppler lidar measurements. Adapted from *Lemonsu et al.* [2006a], with kind permission of Springer Science and Business Media.

version of the TEB scheme [*Lemonsu et al.*, 2004]. Indeed, air temperature measured within urban canyons of Marseille allowed modeled and observed canyon air temperatures to be compared for the first time. The results show that TEB in its original form does not simulate sufficiently rapid ventilation of the air from the canyon. Indeed, the Marseille region is characterized by the presence of strong winds and large net radiative fluxes during summer. When mixing is enhanced (for instance, by modifying canyon aerodynamic resistance), the simulated canyon air temperature is improved. Under sea breeze conditions, cold air advection from the sea increases the temperature gradient between the ground and the atmosphere. As a consequence, the partitioning between sensible heat flux and storage favors the turbulent sensible heat flux, contrary to the results from the Mexico City core, where TEB was initially evaluated [*Masson et al.*, 2002]. Nevertheless, the Marseille city center required specific attention, because their urban parameters are totally different than those usually applied to dense city centers.

4.4.2. Model Validation

[47] The deployment of innovative remote sensors to document at high temporal and spatial resolutions the three-dimensional flow structure was the instrumental core for new methods of validation of high resolution modeling, especially for weak flow dynamics (at most 5–6 m s^{-1}) which has never been done before. *Lemonsu et al.* [2006a] simulated the fine-scale flow with Méso-NH model using nested domains with 250 m horizontal resolution for the finest domain and TEB scheme, similar to the radial resolution of a ground based Doppler (called TWL for transportable wind lidar) deployed at Vallon d'Ol. To do so, similar simulated radial velocity fields are computed from the simulated flow using the relation between the radial velocity and the three components of the wind:

$$v_r = U\cos\phi\,\sin\psi + V\cos\phi\,\cos\psi - w\sin\phi \qquad (2)$$

where U is the zonal wind component, V the meridional wind component, w the vertical wind speed, ϕ the elevation angle and ψ the azimuth angle. Figure 16 shows the comparison between the radial velocities from the TWL (Figure 16, left) and from the model (Figure 16, right) for one vertical scan across the northern district of Marseille, at 190° from the north on 26 June 1001 at 1400 UTC. The TWL data indicate the superimposition of 4 layers (labeled *A*, *B*, *C*, and *D* in Figure 16). In layers *B*, *C* and *D*, the radial velocities are globally negative. Near the surface, the TWL measures positive radial velocities up to 600–700 m asl to a distance of 4.7 km away from the TWL. This layer corresponds to layer *A*. Beyond 4.7 km to the south of Vallon d'Ol, the TWL records negative velocities near the surface. This change of sign of the radial velocity illustrates the convergence between a flow with a northerly component and a flow with a southerly component above the city core [*Delbarre et al.*, 2005; *Augustin et al.*, 2006]. Despite some discrepancies (location of the convergence zone, depth of layer *A*), the numerical model is able for this particular case to reproduce the very fine scale structure of the sea breeze above the city of Marseille, both qualitatively and quantitatively.

[48] Ozone lidars also proved to be an extremely relevant tool to validate chemistry transport models, allowing a new insight on ozone mesoscale variability in the free troposphere. Figure 17 shows the time series of observed ozone values during IOP2 at 1500 m and 3100 m above ground level and the corresponding simulated values obtained with MOCAGE chemistry transport model. Indeed, MOCAGE is the only model used for the ESCOMPTE database analysis which is able to reproducing the observed signal above about 2500 m. Most of the other models are "PBL chemistry models", dedicated to the numerical simulation of air pollution at the surface and within the PBL. Part of the signal observed with the lidars is due to a tropopause fold event that occurred on the Atlantic and that travels up to the

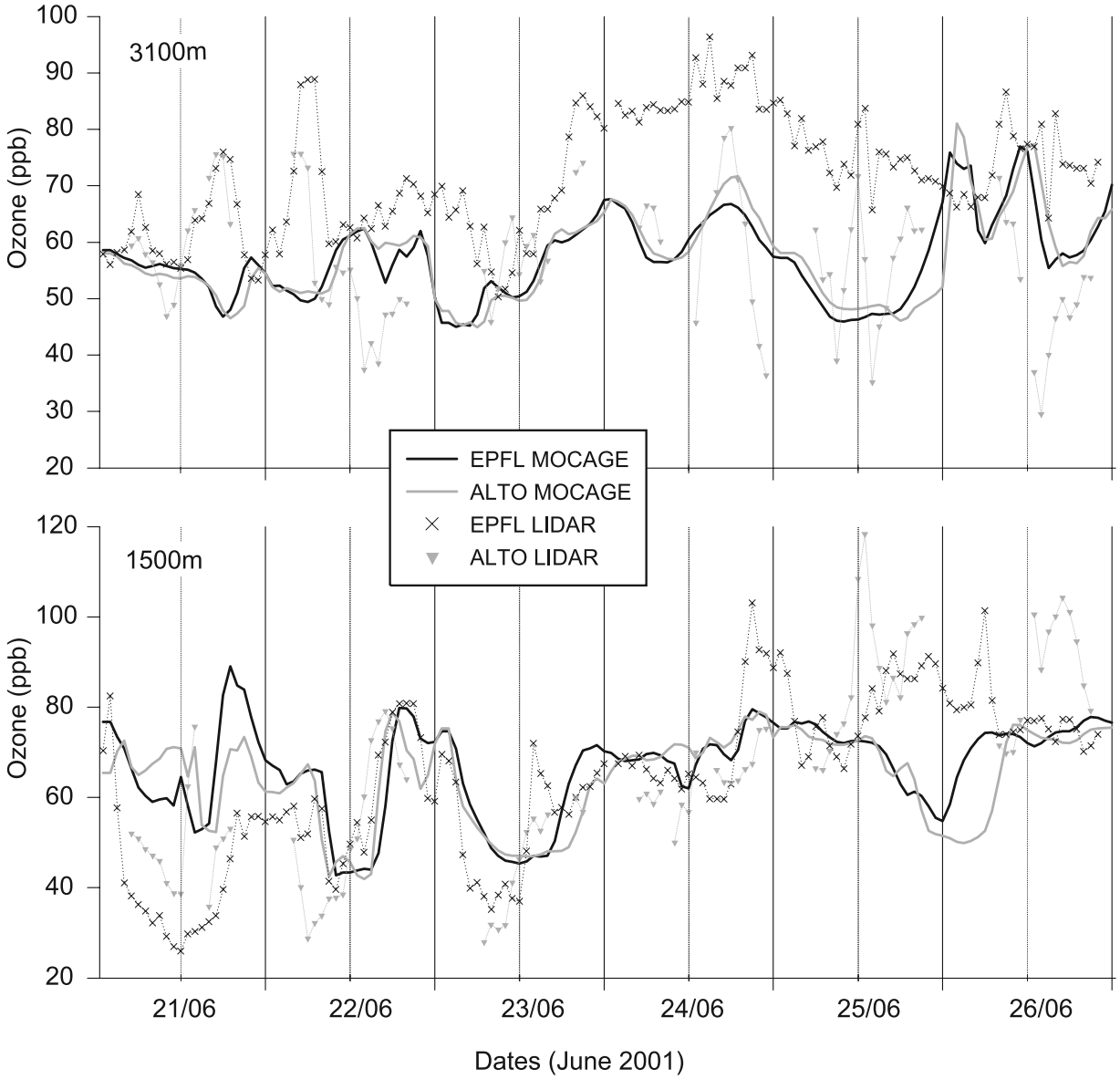

Figure 17. Lidar observations (Saint Chamas (EPFL), crosses, and Aix en Provence (ALTO), triangles) and numerical simulations (MOCAGE chemistry transport model) of ozone time series at Saint Chamas (black) and Aix les Milles (gray), (top) 3100 m and (bottom) 1500 m above ground level. Adapted from *Dufour et al.* [2005].

ESCOMPTE area. Small-scale spatial and temporal variabilities are related to the actual positions of the instruments regarding local emissions and recirculations [*Ancellet and Ravetta*, 2005] and present a diurnal variability that the models can generally quite well capture [*Dufour et al.*, 2005; *Cousin et al.*, 2005]. Interestingly, differences also appear between the two lidars above 2500 m. Such differences, that last over a few days, are rather unexpected at such altitudes given the proximity of the two sites, only located 30 km apart. The model used here is not capable of capturing these differences (the chemistry transport model resolution being approximately 10 km). At 3100 m, the simulated ozone levels are comparable with those measured at Aix les Milles, but with a temporal variability closer to that at Saint Chamas. A much better agreement is observed just above the PBL (1500 m) between the observations at the two sites and between the observations and the model. The differences observed at the mesoscale in the free troposphere requires further investigation, as the 2500–4000 m altitude range is the one where residual pollution layers and upper tropospheric and stratospheric air masses come in contact.

5. Concluding Remarks

[49] Looking back from some distance, the design of the composite observing network may be assessed as quite positive, even though lessons can always be learned. The

composite observing system and the combination of remote sensing and in situ systems produced a wealth of data which allows unprecedented insight into the structure of the sea breeze flow and its contribution to ozone redistribution. The combination of established and novel and highly sophisticated remote sensing instruments with conventional in situ measurements (dense surface network and radiosondes) allowed to capture previously unseen details of the fine structure of the sea breeze and allowed the validation of ultrahigh-resolution numerical research and weather prediction models as well as chemistry transport models. From this work, an operational numerical platform for air quality forecast at fine-scale called AIRES (kilometer-scale resolution, combining the mesoscale model MM5 and the chemistry transport model CHIMERE), has been developed and is currently used by the air quality network AIRMARAIX.

[50] The main findings are that despite the complexity of the terrain, the horizontal transport is mainly driven by the sea breeze and its inland extent by the location of the sea breeze front. The pollutant dilution along its horizontal transport is modulated by the PBL depth which remains shallow near the coast (and thus can contribute to high primary and secondary compound concentrations) and becomes deeper farther inland. The vertical exchanges are predominantly directed from the PBL into the free troposphere, even though entrainment of ozone-rich air within the PBL can be found at sunrise and over the mountains in some occasions. Most of the vertical air mass flux occurs at the sea breeze front, however remaining smaller than the sea breeze induced horizontal mass flux, thus contributing to pollution accumulation just upstream of the sea breeze front. Detrainment at the top of the following breeze within the PBL can not compensate for the upward export. Pollution venting along the slopes is the second contribution to the net vertical export into the free troposphere. It is enhanced by the combination with the sea breeze flow which induces a gravity wave-like oscillatory motion along the slope which affects the time evolution of ozone and nitric oxide concentration. Comparatively to the significant vertical exchanges at the the sea breeze front and along the slopes, entrainment/detrainment at the PBL top is an order of magnitude weaker especially when exchanges of ozone are considered. So, aged tropospheric polluted air masses are not substantially incorporated into the PBL.

[51] Finally, despite the significant progress made in sea breeze understanding, modeling and forecasting thanks to the ESCOMPTE programme, several key issues are still at best partly understood. Among those are mainly the following: (1) A quantitative experimental estimation of the exchanges of pollutant between the PBL and the free troposphere along the mountain slopes has not been conducted during ESCOMPTE because the instrumental setup did not initially aimed at quantifying this contribution, especially in the countryside. (2) The simulation of the polluted ESCOMPTE days with very fine scale numerical models did not succeed in reproducing the oscillating nature of the combined sea breeze and anabatic flow, and its impact on ozone variability along the mountain slope and in the urban area (maybe caused by too coarse resolution of the models or unsuited numerical diffusion scheme in complex terrain, as suggested by *Zängl* [2002]). (3) The model initialization proved to be in some occasions problematic because of a lack representativity of the measurements in the valleys, at hill tops or over very heterogeneous terrain (e.g., near the sea, the Berre pond, the urban zones, etc.) especially during anticyclonic conditions. (4) The numerical simulation of small-scale tropospheric ozone variability, well above the PBL, is currently very challenging as the accurate simulation of these features requires that both long-range transport and detailed local circulations and photochemistry are well accounted for. Further modeling work, involving a hierarchy of coupled chemistry and transport modeling systems that allows to cover the important range of time and spatial scales involved, as well as future observing efforts in the Mediterranean area are needed to further investigate such small-scale variability of free tropospheric ozone.

[52] **Acknowledgments.** The authors would like to thank the three anonymous referees who contributed to improve the manuscript significantly and B. Cros and P. Durand for the coordination of the experiment. In the framework of the French programs PNCA and PRIMEQUAL-PREDIT, ESCOMPTE was performed thanks to funding from the Ministère de l'Écologie et du Développement Durable (MEDD), the Agence de l'Environnement et de la Maîtrise de l'Énergie (ADEME), the Institut National des Sciences de l'Univers (INSU), Météo-France, the Institut National de l'Environnement Industriel et des Risques (INERIS), the German funding agency (BMBF), the Institute for Meteorology and Climate Research (IMK-Karlsruhe), the Joint Research Center (JRC-Ispra), the Swiss Federal Institute of Technology (EPFL-Lausanne), the Centre National d'Études Spatiales (CNES), Électricité de France (EDF), the air quality agencies Airmaraix and Airfobep, the cities of Marseille and Aix en Provence, and the county council of the Bouches-du-Rhône. The flights of the DLR Falcon were funded partly by the CAATER (Co-ordinated Access to Aircraft for Transnational Environmental Research) program of the European Commission. We particularly thank M. P. Lefebvre, who played a crucial role in the delicate organization of the flights.

References

Ancellet, G., and F. Ravetta (2005), Analysis and validation of ozone variability observed by lidar during the ESCOMPTE-2001 campaign, *Atmos. Res.*, *74*, 435–459.

Atkinson, B. W. (1981), *Mesoscale Atmospheric Circulations*, 495 pp., Academic, London.

Augustin, P., H. Delbarre, F. Lohou, B. Campistron, V. Puygrenier, H. Cachier, and T. Lombardo (2006), Investigation of local meteorological events and their relationship with ozone and aerosols during an ESCOMPTE photochemical episode, *Ann. Geophys.*, *24*, 2809–2822.

Aumont, B., A. Jaeker-Voirol, M. Martin, and G. Toupance (1996), Tests of some reduction hypotheses made in photochemical mechanisms, *Atmos. Environ.*, *30*, 2061–2077.

Bastin, S., and P. Drobinski (2005), Temperature, and wind velocity oscillations along a gentle slope during sea-breeze events, *Boundary Layer Meteorol.*, *114*, 573–594.

Bastin, S., and P. Drobinski (2006), Sea breeze induced mass transport over complex terrain in southeastern France: A case study, *Q. J. R. Meteorol. Soc.*, *132*, 405–423.

Bastin, S., P. Drobinski, A. M. Dabas, P. Delville, O. Reitebuch, and C. Werner (2005), Impact of the Rhône and Durance valleys on sea-breeze circulation in the Marseille area, *Atmos. Res.*, *74*, 303–328.

Bastin, S., P. Drobinski, V. Guénard, J. L. Caccia, B. Campistron, A. M. Dabas, P. Delville, O. Reitebuch, and C. Werner (2006), On the interaction between sea-breeze and summer mistral at the exit of the Rhône valley, *Mon. Weather Rev.*, *134*, 1647–1668.

Baumann, K., et al. (2000), Ozone production and transport near Nashville, Tennessee: Results from the 1994 study at New Hendersonville, *J. Geophys. Res.*, *105*, 9137–9151.

Bechtold, P., J. P. Pinty, and P. Mascart (1991), A numerical investigation of the influence of large-scale winds on sea-breeze and inland-breeze-type circulations, *J. Appl. Meteorol.*, *30*, 1268–1279.

Caccia, J. L., V. Guénard, B. Bénech, B. Campistron, and P. Drobinski (2004), Vertical velocity and turbulence aspects during Mistral events as observed by UHF wind profilers, *Ann. Geophys.*, *22*, 3927–3936.

Cheng, W. L. (2002), Ozone distribution in coastal central Taiwan under sea-breeze conditions, *Atmos. Environ.*, *36*, 3445–3459.

Colette, A., G. Ancellet, L. Menut, and S. R. Arnold (2006), A Lagrangian analysis of the impact of transport and transformation on the ozone

stratification observed in the free troposphere during the ESCOMPTE campaign, *Atmos. Chem. Phys.*, *6*, 3487–3503.
Coll, I., S. Pinceloup, P. E. Perros, G. Laverdet, and G. Le Bras (2005), 3D analysis of high ozone production rates observed during the ESCOMPTE campaign, *Atmos. Res.*, *74*, 477–505.
Corsmeier, U., R. Behrendt, P. Drobinski, and C. Kottmeier (2005), The mistral and its effect on air pollution transport and vertical mixing, *Atmos. Res.*, *74*, 275–302.
Cotton, W. R., et al. (2003), RAMS 2001: Current status and future directions, *Meteorol. Atmos. Phys.*, *82*, 5–29.
Cousin, F., P. Tullet, and R. Rosset (2005), Interaction between local and regional pollution during ESCOMPTE 2001: Impact on surface ozone concentration (IOP2a and 2b), *Atmos. Res.*, *74*, 275–302.
Cros, B., et al. (2004), The ESCOMPTE program: An overview, *Atmos. Res.*, *69*, 241–279.
Dalu, G. A., and R. A. Pielke (1989), An analytical study of the sea-breeze, *J. Atmos. Sci.*, *46*, 1815–1825.
Daum, P. H., L. I. Kleinman, D. Imre, L. J. Nunnermacker, Y. N. Lee, S. R. Springston, and L. Newman (2000), Analysis of ozone formation during a stagnation episode in central Tennessee in summer 1995, *J. Geophys. Res.*, *105*, 9107–9119.
Delbarre, H., et al. (2005), Ground-based remote sensing observation of the complex behaviour of the Marseille boundary layer during ESCOMPTE, *Atmos. Res.*, *74*, 403–433.
Drobinski, P., S. Bastin, V. Guénard, J. L. Caccia, A. M. Dabas, P. Delville, A. Protat, O. Reitebuch, and C. Werner (2005), Summer mistral at the exit of the Rhône valley, *Q. J. R. Meteorol. Soc.*, *131*, 353–375.
Drobinski, P., S. Bastin, A. M. Dabas, P. Delville, and O. Reitebuch (2006), Variability of the three-dimensional sea-breeze structure in southeastern France: Observations and evaluation of empirical scaling laws, *Ann. Geophys.*, *24*, 1783–1799.
Dudhia, J. A. (1993), Nonhydrostatic version of the Penn State-NCAR mesoscale model: Validation tests and simulation of an Atlantic cyclone and cold front, *Mon. Weather Rev.*, *121*, 1493–1513.
Dufour, A., M. Amodei, G. Ancellet, and V. H. Peuch (2005), Observed and modelled "chemical weather" during ESCOMPTE, *Atmos. Res.*, *74*, 275–302.
Estoque, M. A. (1962), The sea-breeze as a function of the prevailing synoptic situation, *J. Atmos. Sci.*, *19*, 244–250.
Feliks, Y. (1993), A numerical model for estimation of the diurnal fluctuation of the inversion height due to a sea-breeze, *Boundary Layer Meteorol.*, *62*, 151–161.
Feliks, Y. (2004), Nonlinear dynamics and chaos in the sea and land breeze, *J. Atmos. Sci.*, *61*, 2169–2187.
Fleagle, R. G. (1950), A theory of air drainage, *J. Meteorol.*, *7*, 227–232.
Franois, S., S. Fayet, E. Grondin, and J. L. Ponche (2005), Establishment of the atmospheric emission inventories of the ESCOMPTE program, *Atmos. Res.*, *74*, 5–35.
Fréjafon, E., A. Brut, J. L. Caccia, H. Cachier, C. Jambert, P. Laj, P. Perros, and F. Lohou (2005), Global uncertainties of the 2001 ESCOMPTE field campaign database expected confidence intervals, paper presented at 6th ESCOMPTE Workshop, Marseille, France.
Guénard, V., P. Drobinski, J. L. Caccia, B. Campistron, and B. Bénech (2005), An observational study of the mesoscale mistral dynamics, *Boundary Layer Meteorol.*, *115*, 263–288.
Halley, E. (1686), An historical account of trade winds, and monsoons, observable in the seas between and near the tropics, with an attempt to assign physical cause of said winds, *Philos. Trans. R. Soc.*, *16*, 153–168.
Hasel, M., C. Kottmeier, U. Corsmeier, and A. Wieser (2005), Airborne measurements of turbulent trace gas fluxes and analysis of eddy structure in the convective boundary layer over complex terrain, *Atmos. Res.*, *74*, 381–402.
Hastie, D. R., et al. (1999), Observational evidence for the impact of the lake breeze circulation on ozone concentrations in southern Ontario, *Atmos. Environ.*, *33*, 323–335.
Haurwitz, B. (1947), Comments on the sea-breeze circulation, *J. Meteorol.*, *4*, 1–8.
Kalthoff, N., C. Kottmeier, J. Thürauf, U. Corsmeier, F. Saïd, and E. Fréjafon (2005), Mesoscale circulation systems and ozone concentrations during ESCOMPTE: A case study from IOP 2b, *Atmos. Res.*, *74*, 355–380.
Kitada, T., K. Igarashi, and M. Owada (1986), Numerical analysis of air pollution in a combined field of land/sea-breeze and mountain/valley wind, *J. Clim. Appl. Meteorol.*, *25*, 767–784.
Klemm, O., I. C. Ziomas, D. Balis, P. Suppan, J. Slemr, R. Romero, and L. G. Vyras (1998), A summer air-pollution study in Athens, Greece, *Atmos. Environ.*, *32*, 2071–2087.
Klonecki, A., and H. Levy II (1997), Tropospheric chemical ozone tendencies in CO-CH_4-NO_y-H_2O system: Their sensitivity to variations in environmental parameters and their application to a global chemistry transport model study, *J. Geophys. Res.*, *102*, 21,221–21,237.
Kolev, I., O. Parvanov, B. Kaprielov, E. Doney, and D. Ivanov (1998), Lidar observations of sea-breeze and land-breeze aerosol structure on the Black Sea, *J. Appl. Meteorol.*, *37*, 982–995.
Kolev, I., T. Skakalova, and I. Grigorov (2000), Lidar measurement of aerosol extinction profile in Black Sea coastal zone, *Atmos. Environ.*, *34*, 3813–3822.
Kusuda, M., and P. Alpert (1983), Anti-clockwise rotation of the wind hodograph. Part I: Theoretical study, *Atmos. Environ.*, *32*, 2071–2087.
Lafore, J. P., et al. (1998), The meso-Nh atmospheric simulation system. Part I: Adiabatic formulation and control simulation, *Ann. Geophys.*, *16*, 90–109.
Lasry, F. (2006), Analyse par modélisation tridimensionnelle des processus physico-chimiques déterminant la production d'ozone. Évaluation de l'impact de scénarios d'émissions prospectifs. Application au site ESCOMPTE, Ph.D. thesis, 294 pp., Univ. Paris 12, Créteil, France.
Lelieveld, J., et al. (2002), Global air pollution crossroads over the Mediterranean, *Science*, *298*, 794–799.
Lemonsu, A., C. S. B. Grimmond, and V. Masson (2004), Modelling of the surface energy budget of an old Mediterranean city core: Marseille, *J. Appl. Meteorol.*, *43*, 312–327.
Lemonsu, A., S. Bastin, V. Masson, and P. Drobinski (2006a), Vertical structure of the urban boundary layer over Marseille under sea-breeze condition, *Boundary Layer Meteorol.*, *118*, 477–501.
Lemonsu, A., G. Pigeon, V. Masson, and C. Moppert (2006b), Sea-town interactions over Marseille: 3D urban boundary layer and thermodynamic fields near the surface, *Theor. Appl. Climatol.*, *84*, 171–178.
Liu, K. Y., Z. Wang, and L. F. Hsiao (2002), A modeling of the sea breeze and its impacts on ozone distribution in northern Taiwan, *Environ. Modell. Software*, *17*, 21–27.
Lyons, W. A., and L. E. Olsson (1973), Detailed mesometeorological studies of air pollution dispersion in the Chicago lake breeze, *Mon. Weather Rev.*, *101*, 387–403.
Masson, V. (2000), A physically-based scheme for the urban energy budget in atmospheric models, *Boundary Layer Meteorol.*, *94*, 357–397.
Masson, V., C. S. B. Grimmond, and T. R. Oke (2002), Evaluation of the town energy balance (TEB) scheme with direct measurements from dry districts in two cities, *J. Appl. Meteorol.*, *41*, 1011–1026.
Menut, L., et al. (2000), Measurements and modelling of atmospheric pollution over the Paris area: An overview of the ESQUIF project, *Ann. Geophys.*, *18*, 1467–1481.
Menut, L., I. Coll, and S. Cautenet (2005), Impact of meteorological data resolution on the forecasted ozone concentrations during ESCOMPTE IOP2a and IOP2b, *Atmos. Res.*, *74*, 139–159.
Mestayer, P., et al. (2005), The urban boundary layer field experiment over Marseille UBL/CLU-ESCOMPTE: Experimental set-up and first results, *Boundary Layer Meteorol.*, *114*, 315–365.
Michou, M., P. Laville, D. Sera, A. Fotiadi, P. Bouchou, and V. H. Peuch (2005), Measured and modeled dry deposition velocities over the ESCOMPTE area, *Atmos. Res.*, *74*, 89–116.
Millán, M., R. Salvador, E. Mantilla, and B. Artiñano (1996), Meteorology and photochemical air pollution in southern Europe: Experimental results from EC research projects, *Atmos. Environ.*, *30*, 1909–1924.
Murayama, T., H. Okamoto, N. Kaneyasu, H. Kamataki, and K. Miura (1999), Application of lidar depolarization measurement in the atmospheric boundary layer: Effects of dust and sea-salt particles, *J. Geophys. Res.*, *104*, 31,781–31,792.
Niino, H. (1987), The linear theory of land and sea-breeze circulation, *J. Meteorol. Soc. Jpn.*, *65*, 901–920.
Puygrenier, V. (2006), Étude de la couche limite atmosphérique côtière durant ESCOMPTE 2001: Évaluation et amélioration des performances d'un radar UHF, Ph.D. thesis, 200 pp., Univ. Paul Sabatier, Toulouse, France.
Puygrenier, V., F. Lohou, B. Campistron, F. Saïd, G. Pigeon, B. Bénech, and D. Serca (2005), Investigation on the fine structure of sea-breeze during ESCOMPTE experiment, *Atmos. Res.*, *74*, 329–353.
Rosenthal, J. S., R. A. Helvey, T. E. Battalino, C. Fisk, and P. W. Greiman (2003), Ozone transport by mesoscale and diurnal wind circulations across southern California, *Atmos. Environ.*, *37*, 51–71.
Rotunno, R. (1983), On the linear theory of the land and sea-breeze, *J. Atmos. Sci.*, *40*, 1999–2009.
Saïd, F., U. Corsmeier, N. Kalthoff, C. Kottmeier, M. Lothon, A. Wieser, T. Hofherr, and P. Perros (2005), ESCOMPTE experiment: intercomparison of four aircraft dynamical, thermodynamical, radiative and chemical measurements, *Atmos. Res.*, *74*, 217–252.
Saïd, F., A. Brut, B. Campistron, and F. Cousin (2007), Investigation of the atmospheric boundary layer dynamics during the ESCOMPTE campaign, *Ann. Geophys.*, *25*, 597–622.
Schmidt, F. H. (1947), An elementary theory of the land and sea-breeze circulation, *J. Meteorol.*, *4*, 9–15.

Schmidt, H., C. Derognat, R. Vautard, and M. Beekmann (2001), A comparison of simulated and observed ozone mixing ratios for the summer of 1998 in western Europe, *Atmos. Environ.*, *36*, 6277–6297.

Schultz, P., and T. T. Warner (1982), Characteristics of summertime circulations and pollutant ventilation in the Los Angeles basin, *J. Appl. Meteorol.*, *21*, 672–682.

Simeonov, P., P. Ristori, I. Balin, B. Calpini, and H. Van Den Bergh (2004), A new DIAL based on a N_2 Raman converter for ozone monitoring: Design and application during the ESCOMPTE Campaign, paper presented at XX Quadrennial Ozone Symposium, Int. Ozone Comm., Kos, Greece.

Simpson, J. E. (1994), *Sea Breeze and Local Winds*, 234 pp., Cambridge Univ. Press, New York.

Steyn, D. G. (1998), Scaling the vertical structure of sea breezes, *Boundary Layer Meteorol.*, *86*, 505–524.

Steyn, D. G. (2003), Scaling the vertical structure of sea breezes revisited, *Boundary Layer Meteorol.*, *107*, 177–188.

Taghavi, M., S. Cautenet, and J. Arteta (2005), Impact of a highly detailed emission inventory on modeling accuracy, *Atmos. Res.*, *74*, 65–88.

Traub, M., et al. (2003), Chemical characteristics assigned to trajectory clusters during the MINOS campaign, *Atmos. Chem. Phys.*, *3*, 459–468.

Vautard, R., et al. (2003a), A synthesis of the air pollution over the Paris region (ESQUIF) field campaign, *J. Geophys. Res.*, *108*(D17), 8558, doi:10.1029/2003JD003380.

Vautard, R., et al. (2003b), Paris emission inventory diagnostics from the ESQUIF airborne measurements and a chemistry-transport model, *J. Geophys. Res.*, *108*(D17), 8564, doi:10.1029/2002JD002797.

Vijayakumar, G., K. Parameswaran, and R. Rajan (1998), Aerosols in the atmospheric boundary layer and its association with surface wind speed at a coastal area, *J. Atmos. Sol. Terr. Phys.*, *60*, 1531–1542.

Wakimoto, R. M., and J. L. McElroy (1986), Lidar observations of elevated pollution layers over Los Angeles, *J. Clim. Appl. Meteorol.*, *25*, 1583–1599.

Walsh, J. E. (1974), Sea-breeze theory and applications, *J. Atmos. Sci.*, *31*, 2012–2026.

Wang, T., Y. Y. Wu, T. F. Cheung, and K. S. Lam (2001), A study of surface ozone and the relation to complex wind flow in Hong Kong, *Atmos. Environ.*, *35*, 3203–3215.

Whiteman, C. D., and T. B. McKee (1982a), Breakup of temperature inversions in deep mountain valleys: Part 1. Observations, *J. Appl. Meteorol.*, *21*, 270–289.

Whiteman, C. D., and T. B. McKee (1982b), Breakup of temperature inversions in deep mountain valleys: Part 2. Thermodynamic model, *J. Appl. Meteorol.*, *21*, 290–302.

Zängl, G. (2002), An improved method for computing horizontal diffusion in a sigma-coordinate model and its application to simulations over mountainous topography, *Mon. Weather Rev.*, *130*, 1423–1432.

Zerefos, C. S., et al. (2002), Photochemical activity and solar ultraviolet radiation (PAUR) modulation factors: An overview of the project, *J. Geophys. Res.*, *107*(D18), 8134, doi:10.1029/2000JD000134.

Ziomas, I. C., P. Tzoumaka, D. Balis, D. Melas, C. S. Zerefos, and O. Klemm (1998), Ozone episodes in Athens, Greece: A modelling approach using data from the MEDCAPHOT-TRACE, *Atmos. Environ.*, *32*, 2313–2321.

G. Ancellet, S. Bastin, and A. Colette, Institut Pierre-Simon Laplace, Service d'Aéronomie, Université Pierre et Marie Curie, 4 place Jussieu, F-75252 Paris, France.

P. Drobinski and L. Menut, Laboratoire de Météorologie Dynamique, Institut Pierre-Simon Laplace, Ecole Polytechnique, F-91128 Palaiseau Cédex, France. (philippe.drobinski@aero.jussieu.fr)

A. Brut, B. Campistron, B. Cros, P. Durand, F. Lohou, C. Moppert, V. Puygrenier, and F. Saïd, Laboratoire d'Aérologie, Université Paul Sabatier, 14 avenue E. Belin, F-31400 Toulouse, France.

J. Arteta and S. Cautenet, Laboratoire de Météorologie Physique, Université Blaise Pascal, 24 Avenue des Landais, F-63174 Aubière, France.

P. Augustin and H. Delbarre, Laboratoire de Physico-Chimie de l'Atmosphère, Université du Littoral-Côte d'Opale, 189A avenue Maurice Schumann, F-59140 Dunkerque, France.

J. L. Caccia and V. Guénard, Laboratoire de Sondages Electromagnétiques de l'Environnement Terrestre, Université du Sud Toulon-Var, F-83957 La Garde Cedex, France.

I. Coll and F. Lasry, Faculté des Sciences et Technologie, Laboratoire Inter-Universitaire des Systèmes Atmosphériques, F-94010 Créteil, France.

U. Corsmeier, M. Hasel, N. Kalthoff, and C. Kottmeier, Institut für Meteorologie und Klimaforschung, Forschungszentrum Karlsruhe, Universität Karlsruhe, D-76133 Karlsruhe, Germany.

A. Dabas, A. Dufour, A. Lemonsu, V. Masson, and V. H. Peuch, Centre National de Recherches Météorologiques, Météo-France, 42 avenue G. Coriolis, F-31057 Toulouse, France.

O. Reitebuch, Institut für Physik der Atmosphäre, Deutsches Zentrum für Luft- und Raumfahrt, D-82234 Weßling, Germany.

R. Vautard, Laboratoire des Sciences du Climat et de l'Environnement, Institut Pierre-Simon Laplace, Commisariat à l'Énergie Atomique, F-91191 Gif-sur-Yvette cedex, France.